QCD Precision Measurements and Structure Function Extraction at a High Statistics, High Energy Neutrino Scattering Experiment: NuSOnG

T. Adams[6], P. Batra[4], L. Bugel[4], L. Camilleri[4], J.M. Conrad[9], A. de Gouvêa[12], P.H. Fisher[9], J.A. Formaggio[9], J. Jenkins[12], G. Karagiorgi[9], T.R. Kobilarcik[5], S. Kopp[16], G. Kyle[11], W.A. Loinaz[1], D.A. Mason[5], R. Milner[9], R. Moore[5], J. G. Morfín[5], M. Nakamura[10], D. Naples[13], P. Nienaber[14], F.I Olness[15], J.F. Owens[6], S.F. Pate[11], A. Pronin[3], W.G. Seligman[4], M.H. Shaevitz[4], H. Schellman[12], I. Schienbein[8], M.J. Syphers[5], T.M.P. Tait[2,12], T. Takeuchi[17], C.Y. Tan[5], R.G. Van de Water[7], R.K. Yamamoto[9], J.Y. Yu[15]

[1] *Amherst College, Amherst, MA 01002*
[2] *Argonne National Laboratory, Argonne , IL 60439*
[3] *Central College, Pella IA 50219*
[4] *Columbia University, New York, NY 10027*
[5] *Fermi National Accelerator Laboratory, Batavia IL 60510*
[6] *Florida State University, Tallahassee, FL 32306*
[7] *Los Alamos National Accelerator Laboratory, Los Alamos, NM 87545*
[8] *LPSC, Université Joseph Fourier Grenoble 1, 38026 Grenoble, France*
[9] *Massachusetts Institute of Technology, Cambridge, MA 02139*
[10] *Nagoya University, 464-01, Nagoya, Japan*
[11] *New Mexico State University, Las Cruces, NM 88003*
[12] *Northwestern University, Evanston, IL 60208*
[13] *University of Pittsburgh, Pittsburgh, PA 15260*
[14] *Saint Mary's University of Minnesota, Winona, MN 55987*
[15] *Southern Methodist University, Dallas, TX 75205*
[16] *University of Texas, Austin TX 78712*
[17] *Virginia Tech, Blacksburg VA 24061*

(Dated: June 19, 2009)

We extend the physics case for a new high-energy, ultra-high statistics neutrino scattering experiment, NuSOnG (Neutrino Scattering On Glass) to address a variety of issues including precision QCD measurements, extraction of structure functions, and the derived Parton Distribution Functions (PDFs). This experiment uses a Tevatron-based neutrino beam to obtain a sample of Deep Inelastic Scattering (DIS) events which is over two orders of magnitude larger than past samples. We outline an innovative method for fitting the structure functions using a parameterized energy shift which yields reduced systematic uncertainties. High statistics measurements, in combination with improved systematics, will enable NuSOnG to perform discerning tests of fundamental Standard Model parameters as we search for deviations which may hint of "Beyond the Standard Model" physics.

Contents

I. INTRODUCTION

A. NuSOnG: Precision Structure Functions and Incisive QCD Measurements

The search for new physics at the "Terascale" – energy scales of ~ 1 TeV and beyond – is the highest priority for particle physics.

NuSOnG is a proposed high energy, high statistics neutrino scattering experiment that can search for "new physics" from the keV through TeV energy scales via precision electroweak and QCD measurements.

During its five-year data acquisition period, the NuSOnG experiment could record almost one hundred thousand neutrino-electron elastic scatters, and hundreds of millions of Deep Inelastic Scattering (DIS) events, exceeding the current world data sample by more than an order of magnitude.

This experiment can address concerns related to extraction of structure functions and their derived Parton Distribution Functions (PDFs), investigate nuclear corrections, constrain isospin violation limits, and perform incisive measurement of heavy quarks.

II. DEEP INELASTIC SCATTERING AND PARTON DISTRIBUTION FUNCTIONS

Experiment	ν DIS events	$\bar{\nu}$ DIS events	main target	isoscalar correction
CCFR	0.95M	0.17M	iron	5.67% [4]
NuTeV	0.86M	0.24M	iron	5.74% [5]
NuSOnG	606M	34M	glass	isoscalar

Table I: Comparison of statistics and targets for parton distribution studies in NuSOnG compared to the two past highest statistics DIS neutrino scattering experiments.

Obtaining a high quality model of the parton distribution functions in neutrino and antineutrino scattering is crucial to the NuSOnG electroweak measurements [3]. NuSOnG will go a step beyond past experiments in addressing the systematics of parton distribution functions (PDFs) by making high statistics measurements for neutrino and antineutrino data separately. Table I shows the large improvement in statistics for NuSOnG compared to NuTeV and CCFR, the previous highest statistics experiments. Issues of uncertainties on the nuclear corrections are avoided by extracting PDFs on SiO_2 directly, in similar fashion to the NuTeV Paschos-Wolfenstein (PW) analysis.

The differential cross sections for neutrino and antineutrino CC DIS each depend on three structure functions: F_2, xF_3 and R_L. They are given by:

$$\frac{d^2\sigma^{\nu(\overline{\nu})N}}{dxdy} = \frac{G_F^2 M E_\nu}{\pi\left(1+Q^2/M_W^2\right)^2}\left[F_2^{\nu(\overline{\nu})N}(x,Q^2)\left(\frac{y^2+(2Mxy/Q)^2}{2+2R_L^{\nu(\overline{\nu})N}(x,Q^2)}+1-y-\frac{Mxy}{2E_\nu}\right)\pm xF_3^{\nu(\overline{\nu})N} y\left(1-\frac{y}{2}\right)\right], \quad (1)$$

where $+(-)$ is for $\nu(\overline{\nu})$ scattering. In this equation, x is the Bjorken scaling variable, y the inelasticity, and Q^2 the squared four-momentum transfer. The structure functions are directly related to the PDFs.

The function $xF_3(x,Q^2)$ is unique to the DIS cross section for the weak interaction. It originates from the parity-violating term in the product of the leptonic and hadronic tensors. For an isoscalar target, in the quark-parton model, where $s=\bar{s}$ and $c=\bar{c}$,

$$\begin{aligned} xF_3^{\nu N}(x) &= x\left(u(x)+d(x)+2s(x)\right. \quad (2)\\ &\quad \left.-\bar{u}(x)-\bar{d}(x)-2\bar{c}(x)\right), \\ xF_3^{\bar{\nu}N}(x) &= xF_3^{\nu N}(x)-4x\left(s(x)-c(x)\right). \quad (3)\end{aligned}$$

In past experiments, the average of xF_3 for neutrinos and antineutrinos has been measured. Defining $xF_3 = \frac{1}{2}(xF_3^{\nu N}+xF_3^{\bar{\nu}N})$, at leading order in QCD,

$$xF_{3,LO} = \sum_{i=u,d..} xq_i(x,Q^2) - x\overline{q_i}(x,Q^2). \quad (4)$$

To the level that the sea quark distributions have the same x dependence, and thus cancel, xF_3 can be thought of as probing the valence quark distributions. The difference between the neutrino and antineutrino parity violating structure functions, $\Delta(xF_3) = xF_3^{\nu N} - xF_3^{\bar{\nu}N}$, probes the strange and charm seas. (*Cf.* Sec. VI.)

The function $F_2(x,Q^2)$ appears in both the cross section for charged lepton (e or μ) DIS and the cross section for ν DIS. At leading order,

$$F_{2,LO} = \sum_{i=u,d..} e_i^2(xq_i(x,Q^2)+x\overline{q_i}(x,Q^2)), \quad (5)$$

where e_i is the charge associated with the interaction. In the weak interaction, this charge is unity. For charged-lepton scattering mediated by a virtual photon, e_i is the fractional electromagnetic charge of the quark flavor. Thus $F_2^{\nu N}$ and $F_2^{e(\mu)N}$ are analogous but not identical and comparison yields useful information about specific parton distribution flavors [6] and charge symmetry violation as discussed below. In past neutrino experiments, F_2^{ν} and $F_2^{\bar{\nu}}$ have been taken to be identical and an average F_2 has been extracted, although this is not necessarily true in nuclear targets, as discussed below.

Similarly, $R_L(x,Q^2)$, the longitudinal to transverse virtual boson absorption cross-section ratio, appears in both the charged-lepton and neutrino scattering cross sections. To extract R_L from the cross section, one must bin in the variables x, Q^2 and y. This requires a very large data set. To date, the best measurements for R_L come from charged lepton scattering rather than neutrino scattering [7]. Therefore, neutrino experiments have used charged lepton fits to R_L as an input to the measurements of xF_3 and F_2 [8]. This, however, is just a matter of the statistics needed for a global fit to all of the unknown structure functions in x and Q^2 bins [9]. With the high statistics of NuSOnG, precise measurement of R_L will be possible from neutrino scattering for the first time.

As an improvement on past experiments, the high statistics of NuSOnG allows measurement of up to six structure functions: F_2^{ν}, $F_2^{\bar{\nu}}$, xF_3^{ν}, $xF_3^{\bar{\nu}}$, R_L^{ν} and $R_L^{\bar{\nu}}$. This is done by fitting the neutrino and antineutrino data separately in x, y and Q^2 as described in Eq. (1). The first steps toward fitting all six structure functions independently were made by the CCFR experiment [10], however statistics were such that only xF_3^{ν}, $xF_3^{\bar{\nu}}$, and F_2-average and R-average could be measured, where the average is over ν and $\bar{\nu}$. A global fit of up to six structure functions in NuSOnG would allow separate parameterizations of the underlying PDFs which can account for the nuclear and isospin violation issues discussed below.

In addition to fitting to the inclusive DIS sample, neutrino scattering can also probe parton distributions through exclusive samples. A unique and important case is the measurement of the strange sea through charged current (CC) opposite sign dimuon production. When the neutrino interacts with an s or d quark, it can produce a charm quark that fragments into a charmed hadron. The charmed hadron's semi-leptonic decay (with branching ratio $B_c \sim 10\%$) produces a second muon of opposite sign from the first:

$$\begin{aligned}\nu_\mu \;+\; \mathrm{N} \;\longrightarrow\; \mu^- + c \;+\; \mathrm{X} \\ \hookrightarrow s \;+\; \mu^+ \;+\; \nu_\mu\,. \quad (6)\end{aligned}$$

Similarly, with antineutrinos, the interaction is with an $\overline{s}$ or $\overline{d}$,

$$\begin{aligned}\overline{\nu}_\mu \;+\; \mathrm{N} \;\longrightarrow\; \mu^+ + \overline{c} \;+\; \mathrm{X} \\ \hookrightarrow \overline{s} + \;\mu^- \;+\; \overline{\nu}_\mu\,. \quad (7)\end{aligned}$$

The opposite sign of the two muons can be determined for those events where both muons reach the toroid spectrometer. Study of these events as a function of the kinematic variables allows extraction of the strange sea, the charm quark mass, the charmed particle branching ratio (B_c), and the Cabibbo-Kobayashi-Maskaka matrix element, $|V_{cd}|$.

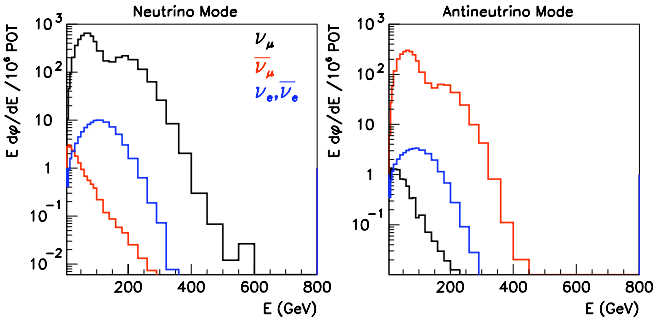

Figure 1: The assumed energy-weighted flux ($E\,d\phi/dE/10^6\,POT$) based on the NuTeV experiment in a) neutrino mode (left) and b) antineutrino mode (right). a) In neutrino mode the fluxes are ordered: upper (black), muon neutrino; middle (blue), electron neutrino and antineutrino; lower (red), muon antineutrino. b) In antineutrino mode the fluxes are ordered: upper (red), muon antineutrino; middle (blue), electron neutrino and antineutrino; lower (black), muon neutrino.

III. EXPERIMENTAL EXTRACTION OF STRUCTURE FUNCTIONS IN NUSONG

A. Description of NuSOnG

The NuSOnG detector was designed to be sensitive to a wide range of neutrino interactions from ν-electron scattering as well as ν-nucleon scattering, though this paper focuses mainly on the latter process. The design has been described in detail in Refs. [3, 11] and so we provide only a brief summary here.

The neutrino beam would be produced via a high energy external proton beam from a high intensity accelerator with energy of $\sim$ 1 TeV. The Fermilab Tevatron is an existing example. The CERN SPS+ [12, 13], which is presently under consideration because of its value to the LHC energy and luminosity upgrades and to a future beta beam, is a second example.

The NuSOnG beam design will be based on the one used by the NuTeV experiment, which is the most recent high energy, high statistics neutrino experiment. The experiment would use 800 GeV protons on target followed by a quad-focused, sign-selected magnetic beamline. The beam flux, shown in Fig. 1, has very high neutrino or antineutrino purity ($\sim$98%) and small ν_e contamination ($\sim$2%) from kaon and muon decay. Using an upgraded Tevatron beam extraction it is expected that NuSOnG could collect 5×10^{19} protons/yr, an increase by a factor of 20 from NuTeV. With this high intensity, such a new facility would also produce a neutrino beam from the proton dump having a sizable fraction of tau neutrinos for study.

The baseline detector design is composed of a fine-grained target calorimeter for electromagnetic and hadronic shower reconstruction followed by a toroid muon spectrometer to measure outgoing muon momenta. The target calorimeter will be composed of 2,500 2.5 cm $\times$ 5 m $\times$ 5 m glass planes interspersed with proportional tubes or scintillator planes. This gives a target which is made of isoscalar material with fine 1/4 radiation length sampling. The detector will be composed of four target sections each followed by muon spectrometer sections and low mass decay regions to search for long-lived heavy neutral particles produced in the beam. The total length of the detector is $\sim$200 m and the fiducial mass for the four target calorimeter modules will be 3 kiloton which is 6 times larger than NuTeV or CHARM II. Figure 2 shows a simulated ν_μ charged current event in the detector.

B. Description of NuSOnG Calibration Beam

The requirements for NuSOnG calibration beam would be similar to those of NuTeV. Tagged beams of hadrons, electrons, and muons over a wide energy range (5-200 GeV) would be required. The calibration beam will have the ability to be steered over the transverse face of the detector in order to map the magnetic field of each toroid with muons. Steering for hadrons and electrons would be less crucial than it was in NuTeV's case, but would still be useful.

The calibration beam can be constructed with a similar design to NuTeV. Upstream elements were used to select hadrons, electrons, or muons. An enhanced beam of electrons was produced by introducing a thin lead radiator into the beam and detuning the portion of the beam downstream of the radiator. A radiator was also used in the nominal beam tune to remove electrons. Particle ID (a threshold Cerenkov and TRDs) was incorporated in the spectrometer and used to tag electrons when running at low energy. A pure muon beam was produced by introducing a 7 m long beryllium filter in the beam as an absorber.

The NuTeV calibration spectrometer determined incoming particle momenta with a precision of better than 0.3% absolute [14]. The NuSOnG goal for calibration-beam precision would be to measure energy scales to a precision of about 0.5%, and we demonstrate (in later text of this paper) that this can be improved with fits to neutrino data.

For comparison, using the calibration beam, NuTeV achieved 0.43% precision on absolute hadronic energy scale and 0.7% on absolute muon energy scale (dominated by the ability to accurately determine the toroid map). Precise knowledge of the muon energy scale is especially important in order to achieve high measurement accuracy on the neutrino fluxes using the low-ν method. For example, a 0.5% precision on muon energy scale translates into about a 1% precision on the flux. Both energy scales are important for precision structure function measurements, and were the largest contributions to structure function measurement uncertainties in NuTeV [15].

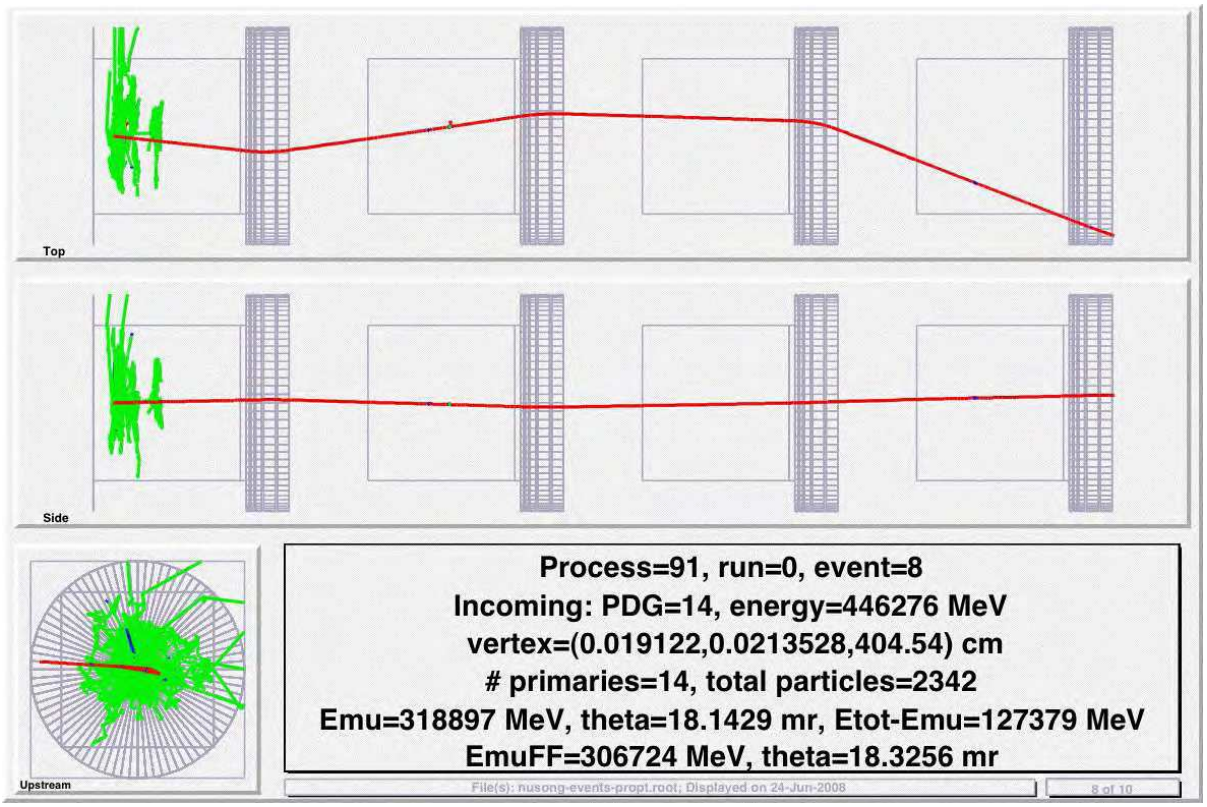

Figure 2: A simulated muon neutrino, charged current event in the NuSOnG detector.

C. Experimental Extraction of Structure Functions in NuSOnG

The high statistics of the NuSOnG experiment makes it possible to extract the structure functions directly from the y-distributions within bins of $\left(x, Q^2\right)$. Previous lower-statistics high-energy neutrino experiments either extracted structure functions by comparing the number of ν versus $\overline{\nu}$ events in an $\left(x, Q^2\right)$ bin [4], or by extracting the cross-sections $d\sigma/dy$ within the $\left(x, Q^2\right)$ bin and fitting for the structure functions using Equation (1) [15]. Either method assumes a value for $R_L = \sigma_L/\sigma_T$ as measured by other experiments [16], and depends on a measurement of the strange sea from dimuon events [17, 18]. With sufficient statistics, we can explore the possibility of measuring $xF_3^{\nu}\left(x, Q^2\right)$, $xF_3^{\overline{\nu}}\left(x, Q^2\right)$, $F_2\left(x, Q^2\right)$, and $R\left(x, Q^2\right)$ from the same data [10].

Let us denote Eq. (1) as a function of the structure functions by $d\sigma^{\nu(\overline{\nu})}\left(xF_3, F_2, R\right)$, where the $\left(x, Q^2\right)$-dependence is assumed and where the structure functions can be different for neutrinos and antineutrinos. A sample of Monte Carlo events, $N_{MC,gen}^{\nu(\overline{\nu})}$, is generated using an assumed set of structure functions for the cross-section: $d\sigma^{\nu,\overline{\nu}}\left(xF_3^{gen}, F_2^{gen}, R^{gen}\right)$. One can then fit for the structure functions in each $\left(x, Q^2\right)$ bin by minimizing

$$\chi^2 = \sum_{\nu,\overline{\nu}} \sum_{y-\text{bins}} \frac{\left(N_{data}^{\nu(\overline{\nu})} - N_{MC,pred}^{\nu(\overline{\nu})}\left(SF_{fit}\right)\right)^2}{N_{data}^{\nu(\overline{\nu})}}, \tag{8}$$

where $N_{MC,pred}^{\nu(\overline{\nu})}\left(SF_{fit}\right)$, the reweighted Monte-Carlo events in an $\left(x, Q^2, y\right)$ bin, is given by

$$N_{MC,pred}^{\nu(\overline{\nu})}\left(SF_{fit}\right) = \sum_{\substack{\nu(\overline{\nu}) \text{ events in} \\ \left(x,y,Q^2\right) \text{ bin}}} \frac{d\sigma^{\nu(\overline{\nu})}\left(xF_3^{fit}, F_2^{fit}, R^{fit}\right)}{d\sigma^{\nu(\overline{\nu})}\left(xF_3^{gen}, F_2^{gen}, R^{gen}\right)} N_{MC,gen}^{\nu(\overline{\nu})}\left(SF_{gen}\right), \tag{9}$$

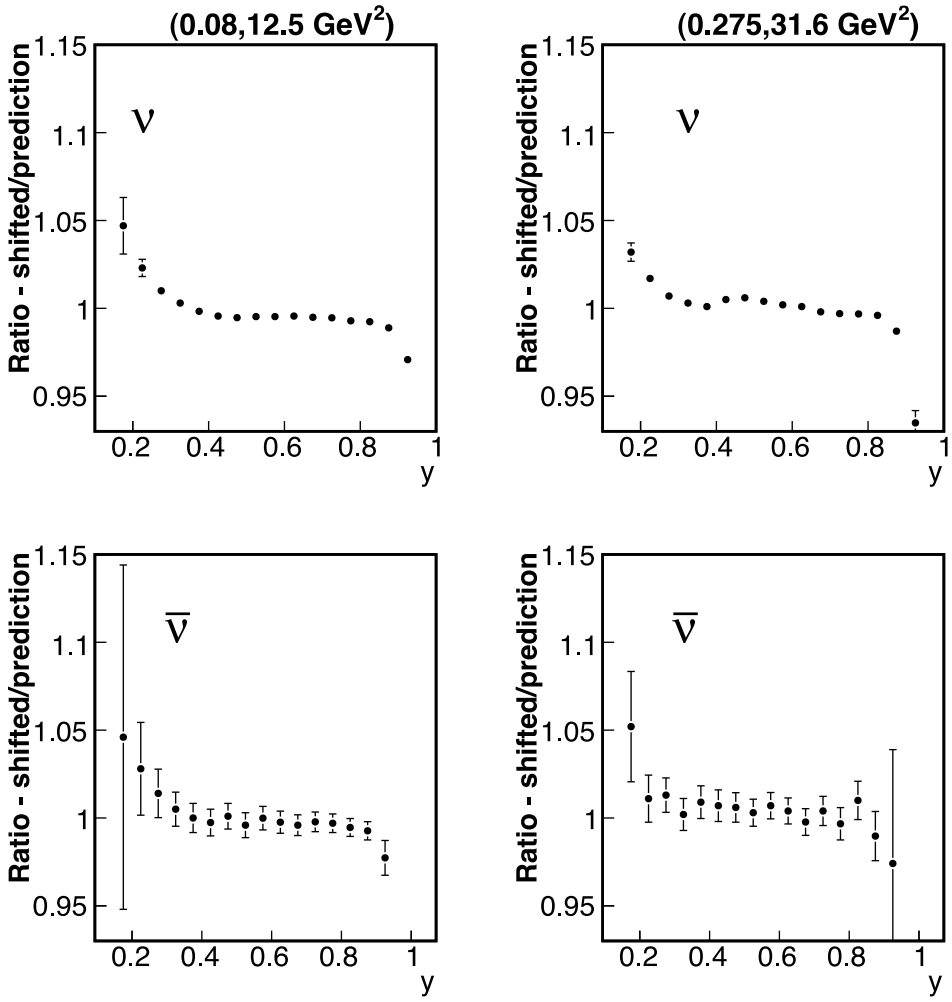

Figure 3: Fractional change in number of events for two characteristic (x, Q^2) bins as a function of y. The fractional change comes from scaling the energy of each event by a factor of 1.005.

$N_{data}^{\nu(\overline{\nu})}$ is the number of ν or $\overline{\nu}$ data events in the $\left(x, y, Q^2\right)$ bin, and $N_{MC,gen}^{\nu(\overline{\nu})}$ is the number of Monte-Carlo events generated in the $\left(x, y, Q^2\right)$ bin. $xF_3^{fit}\left(x, Q^2\right)$, $F_2^{fit}\left(x, Q^2\right)$, and $R^{fit}\left(x, Q^2\right)$ are the fit parameters in the χ^2-minimization of Eq. (8). In principle they can be fit separately for ν and $\overline{\nu}$ structure functions. Here we will concentrate on the measurement ox f up to four separate structure functions, $\Delta xF_3\left(x, Q^2\right) = xF_3^{\nu}\left(x, Q^2\right) - xF_3^{\overline{\nu}}\left(x, Q^2\right)$, $xF_3^{avg} = (xF_3^{\nu} + xF_3^{\overline{\nu}})/2$, $F_2\left(x, Q^2\right)$, and $R\left(x, Q^2\right)$ where we assume that $F_2\left(x, Q^2\right)$ and $R\left(x, Q^2\right)$ are the same for neutrinos and antineutrinos i.e. $F_2\left(x, Q^2\right) = F_2^{\nu}\left(x, Q^2\right) = F_2^{\overline{\nu}}\left(x, Q^2\right)$ and $R\left(x, Q^2\right) = R^{\nu}\left(x, Q^2\right) = R^{\overline{\nu}}\left(x, Q^2\right)$.

D. Fitting for ΔxF_3

We have studied the extraction of the structure function from the 600 million neutrino and 33 million antineutrino deep inelastic scattering events expected in the full NuSOnG data set. The dominant systematic error comes from the measurement of the muon momentum in the toroidal spectrometer. At NuTeV, the systematic uncertainty was 0.7% and we assume NuSOnG will achieve 0.5%. Our studies are carried out by fitting the y-distribution in each x, Q^2 bin for F_2, the average value of $xF_3 = xF_3^{avg} = (xF_3^{\nu} + xF_3^{\overline{\nu}})/2$, $\Delta xF_3 = xF_3^{\nu} - xF_3^{\overline{\nu}}$,and R. In the first set of studies, $R(x, Q^2)$ is set equal to the measured value[16] and fits are done to the three structure functions, F_2, xF_3^{avg}, and ΔxF_3.

Our fitting procedure begins with a sample of Monte Carlo generated events, $N^{gen}(x, Q^2, y)$, sampled from

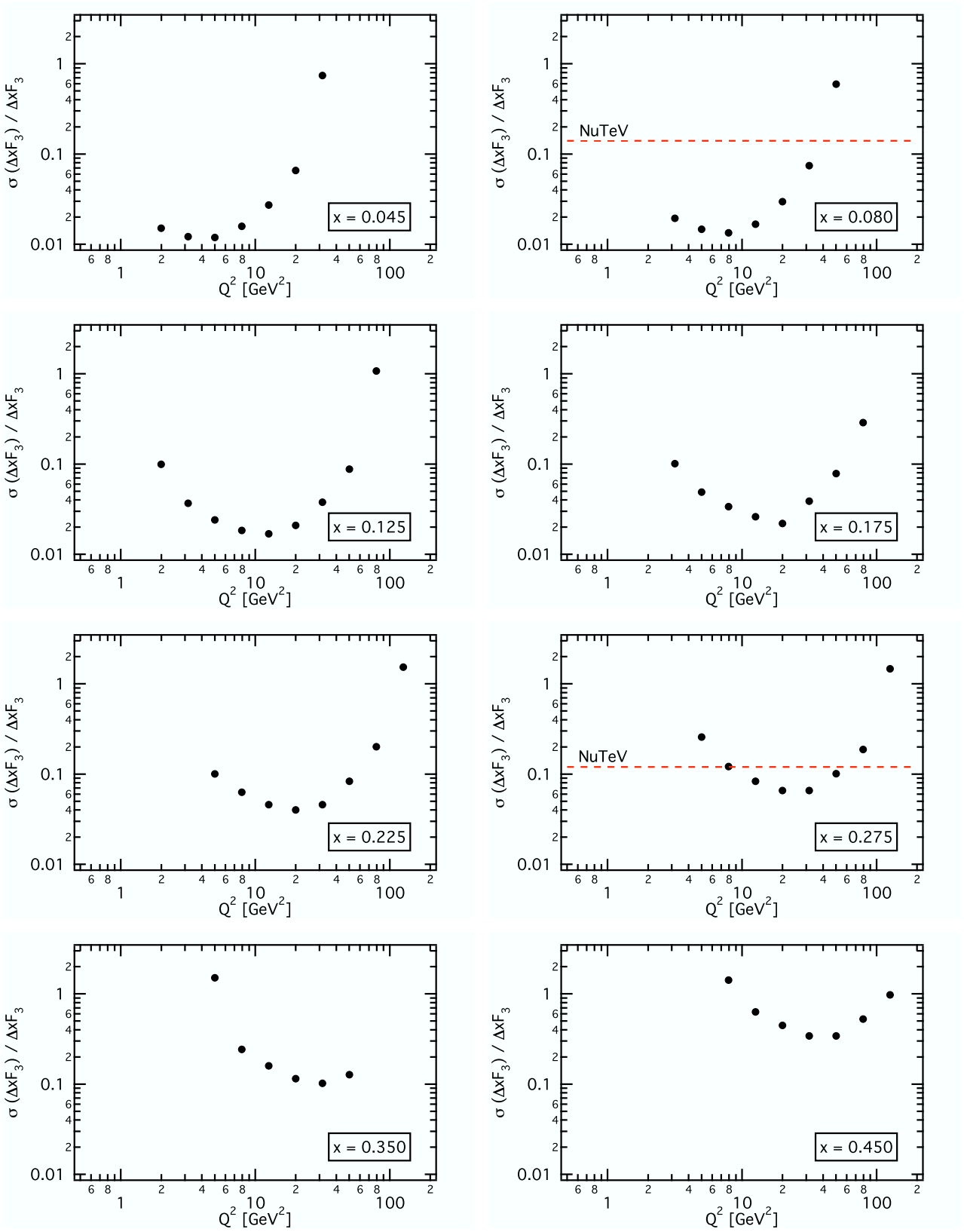

Figure 4: Fractional uncertainty for the fit value of ΔxF_3 in different x bins as a function of Q^2. The fit is to multiple x and Q^2 bins extracting the three structure functions, F_2,xF_3^{avg} and ΔxF_3. For each of the fits, a global set of energy scale parameters is also determined from the fit. The dotted lines show the fractional error for the NuTeV 2μ measurement.

the CCFR structure functions and the nominal value for ΔxF_3 from NuTeV. We fit in bins of (x, Q^2) as a function of y and obtain the fit spectra by reweighting the original sample:

$$N^{fit}(x,Q^2,y) = \frac{F_2^{fit}(x,Q^2)(2-2y+y^2/(1+R)) \pm xF_3^{fit}(x,Q^2)(1-(1-y)^2)}{F_2^{nom}(x,Q^2)(2-2y+y^2/(1+R)) \pm xF_3^{nom}(x,Q^2)(1-(1-y)^2)} N^{gen}(x,Q^2,y).$$

where the upper sign is for neutrinos and the lower for anti-neutrinos. In order to study the effects of the systematic energy scale shift, we produce a Monte Carlo sample where the muon energy scale is shifted by 0.5%, $E_\mu^{meas} = 1.005 E_\mu^{true}$, for each event. The fractional change in the number of events in each bin due to the energy scale shift is shown in Fig. 3.

This shifted event distribution, $N^{shift}(x,Q^2,y)$, is then used to carry out a three parameter fit to Eq. 8 where F_2, xF_3^{avg}, and ΔxF_3 are varied. Large shifts in ΔxF_3 result. For example, the shift from the input value in the $(x,Q^2) = (0.08, 12.6 GeV^2)$ bin is 19.01% and the shift in other bins is even larger.

The effects of the energy scale uncertainty can be practically eliminated by including energy scale shift parameters in the fit. A muon energy scale change shifts the events in the various y-bins by an amount that is not consistent with that expected from changes in the structure functions. Therefore, fits to the y-distributions can isolate the effects of an energy scale shift and significantly reduce the structure function uncertainty from this systematic error. To estimate the systematic error reduction for this technique, three additional energy scale parameters are introduced in the fit to the y-distributions. These three parameters are used to produce an energy scale shift parameterization in each (x,Q^2,y) bin given by

$$E_{\mu scale} = E_{\mu scale1} + E_{\mu scale2} E_\mu + E_{\mu scale3} E_\mu^2.$$

The updated prediction for the number of events in a given (x,Q^2,y) bin is

$$\begin{aligned} N_{pred}^{\nu(\overline{\nu})}(SF_{fit}) &= N_{MC,pred}^{\nu(\overline{\nu})}(SF_{fit}) \\ &+ E_{\mu scale}\left(N^{shift}(x,Q^2,y) - N^{gen}(x,Q^2,y)\right), \end{aligned} \quad . \tag{10}$$

and the χ^2 used in the minimization similar to Eq. 8 with the addition of pull terms associated with the three energy scale parameters

$$\begin{aligned} \chi^2 &= \sum_{\nu,\overline{\nu}} \sum_{y-\text{bins}} \frac{\left(N_{data}^{\nu(\overline{\nu})} - N_{pred}^{\nu(\overline{\nu})}(SF_{fit})\right)^2}{N_{data}^{\nu(\overline{\nu})}} \\ &+ E_{\mu scale1} + \frac{E_{\mu scale2}}{(0.02)^2} + \frac{E_{\mu scale3}}{(0.0002)^2}. \end{aligned} \tag{11}$$

These pull terms correspond to an energy scale uncertainties of about 0.5% for muon energy values averaging between 50 and 70 GeV. This fitting technique renders the systematic error from the scale shift to be small in comparison with the statistical error. For example, in the bin $(x,Q^2) = (0.275,\ 32\ \text{GeV}^2)$ bin, the systematic error for ΔxF_3 is 0.3% while the statistical error is 10%; the value of the $E_{\mu scale1}$ parameter is also determined to about 10%.

In the ultimate analysis, the fit will be carried out simultaneously over all x and Q^2 bins with one set of energy scale parameters. We have studied this using eight x bins and six to eight Q^2 bins. Figure 4 shows the fractional error on ΔxF_3 for different x bins as a function of Q^2. In general, we believe NuSOnG can measure ΔxF_3 over most of the (x,Q^2) range to better than 10%; in many cases around 3%. Typical values for NuTeV are shown in two x bins in Fig. 4. Since more than one (x,Q^2) bin is being used to determine the energy scale shift parameters, the value of the $E_{\mu scale1}$ parameter can also determined to about 3% from these fits.

Simulation studies have also been made to estimate the uncertainties associated with doing fits to extract the four structure functions, F_2, xF_3^{avg}, ΔxF_3,and R. The procedure is the same as used for the three structure function fits where the χ^2 in Eq. 11 is minimized simultaneously over a number of x and Q^2 bins with one set of energy scale parameters. In this case, the ΔxF_3 and R_{long} structure functions can be determined to between 5% and 20% for most of the x and Q^2 range as shown in Figs. 5 and 6. The simulated R_{long} measurements are shown in Fig. 7 along with previous measurements.[16] As indicated from this figure, the capabilities of the NuSOnG to measure R_{long} is much more precise that any previous experiment.

In summary, due to the very high statistics of a NuSOnG type experiment, an almost complete set of structure functions over a broad range of x and Q^2 can be extracted from the data without introducing theoretical or experimental approximations. Further, systematic uncertainties that have limited the precision of previous structure function measurements can be eliminated by including fits to these uncertainties in the extraction procedure. We believe that with these techniques the structure function measurements will be statistics limited even for NuSOnG.

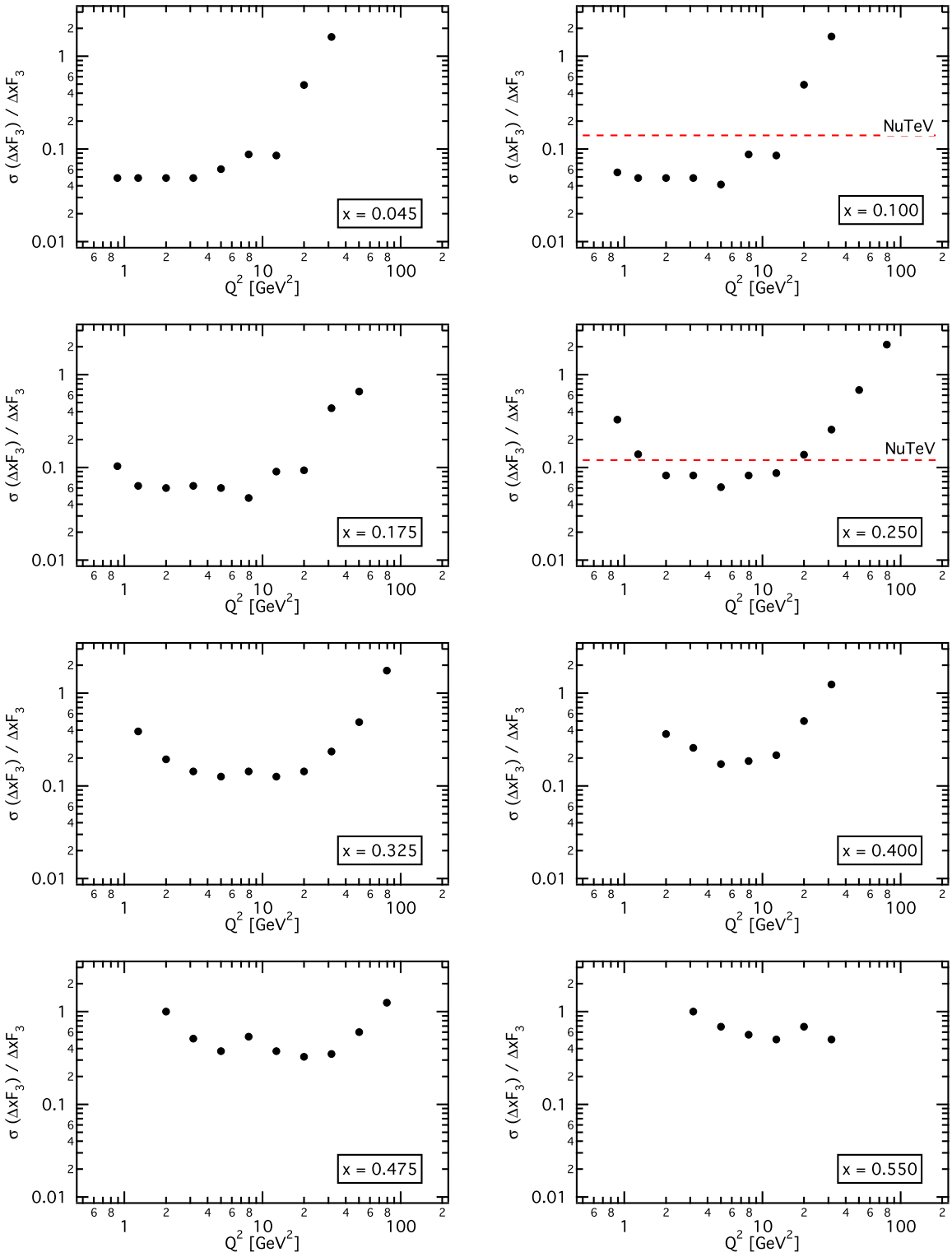

Figure 5: Fractional uncertainty for the fit value of ΔxF_3 in different x bins as a function of Q^2. The fit is to multiple x and Q^2 bins extracting the four structure functions, F_2,xF_3^{avg}, ΔxF_3, and R. For each of the fits, a global set of energy scale parameters is also determined.

IV. NUCLEAR EFFECTS

Historically, neutrino experiments have played a major role in expanding our understanding of parton distribution functions through high statistics experiments such as CCFR [8], NuTeV [8, 15, 19], and CHORUS [20]. However, the high statistics extract a price since the large event samples require the use of nuclear targets – iron in the case of both CCFR and NuTeV and lead in the case of the Chorus experiment. The problem is that if one wants to extract information on *nucleon* PDFs, then the effects of the nuclear targets must first be removed. NuSOnG can provide key measurements which will improve these corrections.

Charged lepton deep inelastic scattering has been measured on a wide range of targets. The most simplistic expectation for the structure functions might be that they would simply be given by an average of the appropriate number of proton and neutron results as in

$$F_2^A(x,Q^2) = \frac{Z}{A}F_2^P(x,Q^2) + \frac{A-Z}{A}F_2^n(x,Q^2).$$

However, the results from a wide range of experiments show a much more complex behavior for the structure functions on nuclei. The typical behavior of the ratio of $F_2^A(x,Q^2)$ to $F_2^d(x,Q^2)$ where d denotes a deuterium target shows four distinct regions as sketched in Fig. 8.

At small x the ratio dips below one in what is called the shadowing region. At somewhat larger values of x the ratio rises above one in the antishadowing region. At still larger values of x the ratio again falls below one in the EMC region. Finally, as x approaches one, Fermi motion smearing causes a significant rise in the ratio.

This behavior shows only a modest dependence on A for values above beryllium, with the shape remaining qualitatively the same and the amount of the suppression at $x \approx 0.6$ increasing slowly with $\log(A)$. Furthermore, there is little, if any, observed dependence on Q^2. These features are summarized nicely in the results shown in Ref. [21].

The mechanisms of nuclear scattering have also been studied theoretically. These mechanisms appear to be different for small and large Bjorken x as viewed from the laboratory system. Bjorken x is defined as $x = Q^2/2M\nu$, where ν and $\boldsymbol{q}$ are energy and momentum transfer to the target and $Q^2 = \boldsymbol{q}^2 - \nu^2$. The physical quantity which is responsible for the separation between large and small x regions is a characteristic scattering time, which is also known as Ioffe time (or length) $\tau_I = \nu/Q^2$ [22]. If τ_I is smaller than the average distance between bound nucleons in a nucleus then the process can be viewed as incoherent scattering off bound nucleons. This happens at larger $x(> 0.2)$.

A. Nuclear effects at small x

We expect to find a difference between charged-lepton nucleus and neutrino nucleus scattering at small-x because the space-time pictures for the two processes are different in this region. The underlying physical mechanism in the laboratory reference frame can be sketched as a two-stage process. At the first stage, the virtual photon γ^*, or W^* or Z^* in case of neutrino interactions, fluctuates into a quark-gluon (or hadronic) state. In the second stage, this hadronic state then interacts with the target. The uncertainty principle allows an estimate of the average lifetime of such hadronic fluctuation as

$$\tau = \frac{2\nu}{m^2+Q^2} = \frac{1}{x\,M}\,\frac{Q^2}{m^2+Q^2}, \qquad (12)$$

where m is invariant mass of hadrons into which the virtual boson convert, and M is the proton mass. The same scale τ also determines characteristic longitudinal distances involved in the process. At small x, τ exceeds the average distance between bound nucleons. For this reason coherent multiple interactions of this hadronic fluctuation in a nucleus are important in the small-x kinematical region. It is well known that the nuclear shadowing effect for structure functions is a result of coherent nuclear interactions of hadronic fluctuations of virtual intermediate boson. [1]

For neutrino interactions which are mediated by the axial-vector current, the fluctuation time τ is also given by Eq. 12. However, as was argued in Ref. [24], the fluctuation and coherence lengths are not the same in this case. In particular, the coherence length is determined by the pion mass m_π in Eq. 12 because of the dominance of off-diagonal transitions like $a_1 N \to \pi N$ in nuclear interactions. Since the pion mass is much smaller than typical masses of intermediate hadronic states for the vector current (m_ρ, m_ω, etc.), the coherence length L_c of intermediate states of the axial current at low Q^2 will be much larger than L_c of the vector current. A direct consequence of this observation is the early onset of nuclear shadowing in neutrino scattering at low energy and and low Q^2 as compared with the shadowing in charged-lepton scattering. The basic reason for this earlier onset and different behavior in the transition region is the difference in the correlation lengths of hadronic fluctuations of the vector and axial-vector currents. This is also illustrated by observing that for a given Q^2, the cross-section suppression due to shadowing occurs for much lower energy transfer (ν) in neutrino interactions than for charged leptons.

[1] For a recent review of nuclear shadowing see, e.g., [23].

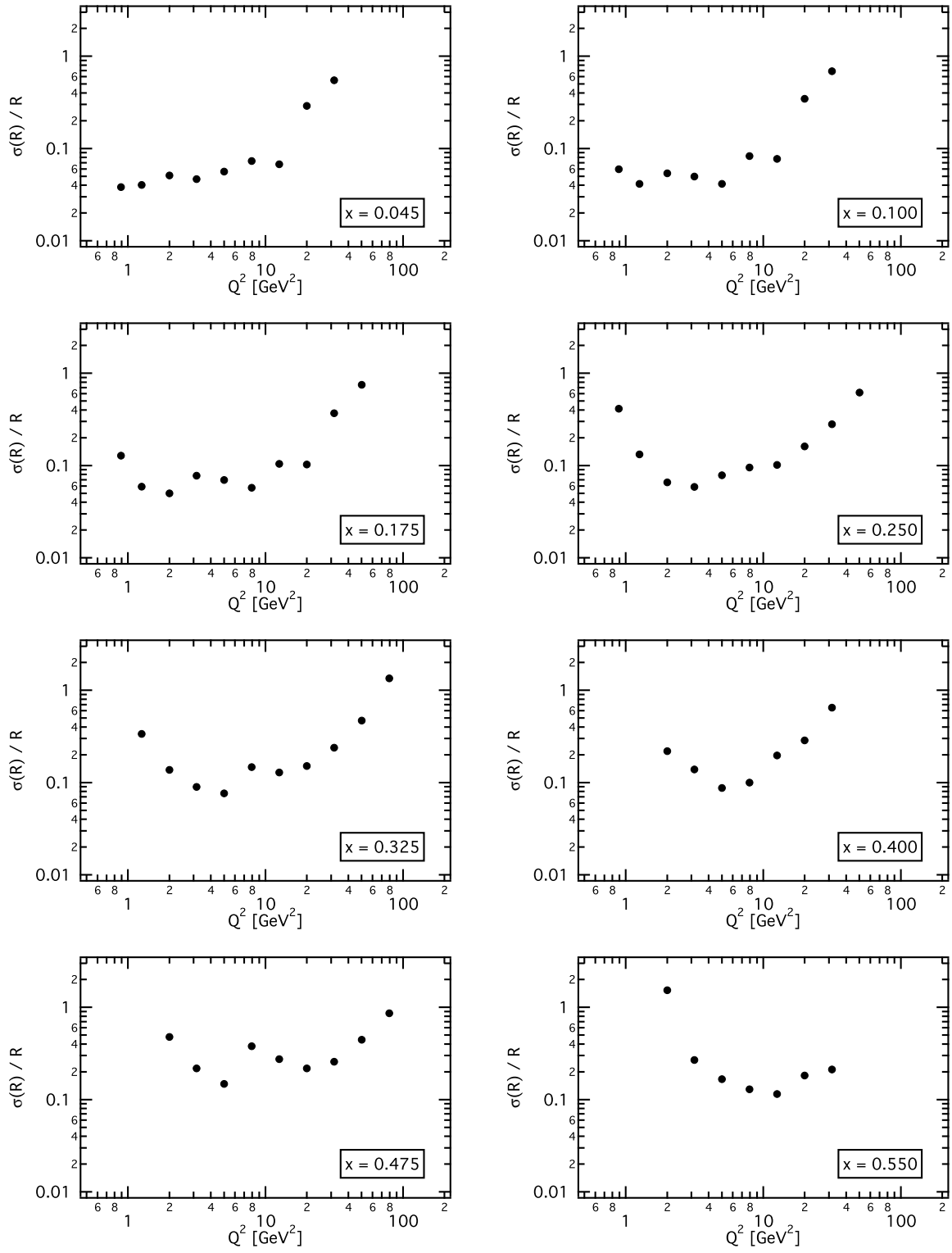

Figure 6: Fractional uncertainty for the fit value of R in different x bins as a function of Q^2. The fit is to multiple x and Q^2 bins extracting the four structure functions, F_2,xF_3^{avg}, ΔxF_3, and R. For each of the fits, a global set of energy scale parameters is also determined.

B. Nuclear Effects in Neutrino Interactions

As there has been no systematic experimental study of ν and $\overline{\nu}$ nucleus interactions, one must then rely on theoretical models of the nuclear corrections. This is an unsatisfactory situation since one is essentially measuring quantities sensitive to the convolution of the the desired PDFs and unknown – or model dependent – nuclear corrections.

As noted above, theoretically there are substantial differences between charged lepton and neutrino interactions on the same nucleus. There are other expected differences for neutrinos. For example, the relative nuclear shadowing effects for the structure function F_3 is predicted to be substantially different from that for F_2 [25]. This is because the structure function F_3 describes the correlation between the vector and the axial-vector current in neutrino scattering. In terms of helicity cross sections, the structure function F_3 is given by the cross section asymmetry between the left- and right-polarized states of a virtual W boson. It is known that such a difference of cross sections is strongly affected by Glauber multiple scattering corrections in nuclei. [26, 27, 28] This causes an enhanced nuclear shadowing effect for the structure function F_3.

It is important to experimentally address the question of nuclear effects in neutrino scattering so that the neutrino data can be used in proton fits without bringing in substantial nuclear uncertainties. For example, in a recent analysis [29] the impact of new neutrino data on global fits for PDFs was assessed. The conclusion reached in this analysis was that the uncertainties associated with nuclear corrections precluded using the neutrino data to constrain the nucleon PDFs. If NuSOnG can address these uncertainties, then the neutrino data can play an even more prominent role in the global fits to the proton PDF.

Furthermore, nuclear effects are interesting in their own right. Parameterizations of nuclear PDFs on various targets exist in the literature. However, there is no universally accepted model which describes these nuclear corrections over the entire range of x from first principles. This makes it difficult to generalize the above behavior observed in charged lepton DIS to DIS with ν or $\overline{\nu}$ beams. Models such as that in Ref. [30] exist, but to date there have been no high statistics studies of ν or $\overline{\nu}$ DIS over a wide range of nuclear targets with which to test them.

A study presented in Ref. [29] examined the role of new lepton pair production data from E-866 and new neutrino DIS data from the NuTeV and CHORUS collaborations in global fits for nucleon PDFs. For the actual fitting of the PDFs it was necessary to include nuclear corrections for the neutrino and antineutrino cross sections and the model of Ref. [30] was used. As a byproduct of that analysis, it was possible to compare a reference fit, obtained without using data on nuclear targets, to the neutrino and antineutrino data in order to obtain an estimate of what the nuclear corrections should look like. This comparison is shown in Fig. 9.

This figure shows some results from Ref. [29] in the form of "data/theory" averaged over Q^2 and presented versus x. The results are from a global fit but are plotted *without* the model-dependent nuclear corrections which were used in the fit (the neutrino data were *not* used in the reference fit.) It is notable that the overall pattern of deviations shown in Fig. 9 are, in general, similar to that seen in charged lepton DIS as sketched in Fig.8. However, the deviations from unity are perhaps smaller. At high x, the effect of Fermi smearing is clear. At moderate x the EMC effect is observable. It is interesting to note that there is no clear indication of a turnover at low x in the shadowing region for ν data. Also, note the striking similarity between the ν and $\overline{\nu}$ results. This appears to imply that the differences in the nuclear effects between neutrino and antineutrino DIS are small. As discussed later, when we consider $\Delta x F_3$ and isospin violation, it is crucial to model differences in the nuclear effects between ν and $\bar{\nu}$ scattering as a function of x.

To make progress in understanding nuclear corrections in neutrino interactions, access to high statistics data on a variety of nuclear targets will be essential. This will allow the A-dependence to be studied as a function of both x and Q^2, as has been done in charged lepton deep inelastic scattering. PDFs from global fits without the neutrino data can then be used to make predictions to be compared with the A-dependent ν and $\overline{\nu}$ cross sections, thereby allowing the nuclear corrections to be mapped out for comparison with theoretical models.

The primary target of NuSOnG will be SiO_2. However, we can investigate a range of A-values by replacing a few slabs of glass with alternative target materials: C, Al, Fe, and Pb. This range of nuclear targets would both extend the results of Minerva to the NuSOnG kinematic region, and provide a check (via the Fe target) against the NuTeV measurement.

Given the NuSOnG neutrino flux, we anticipate $58k$ ν-induced and $30k$ $\bar{\nu}$-induced CC DIS events per ton of material. A single ton would be sufficient to extract $F_2(x)$ and $xF_3(x)$ averaged over all Q^2; a single 5 m$\times$5 m$\times$2.54 cm slab of any of the above materials will weigh more than that. The use of additional slabs would permit further extraction of the structure functions into separate (x, Q^2) bins as was done in the NuTeV analysis, at the potential expense of complicating the shower energy resolution in the sub-detectors containing the alternative targets; this issue will be studied via simulation.

Table II shows that two 50-module stacks would be sufficient to accumulate enough statistics on alternative nuclear targets for a full structure-function extraction for each material. However, for basic cross-section ratios in x, a single slab of each would suffice.

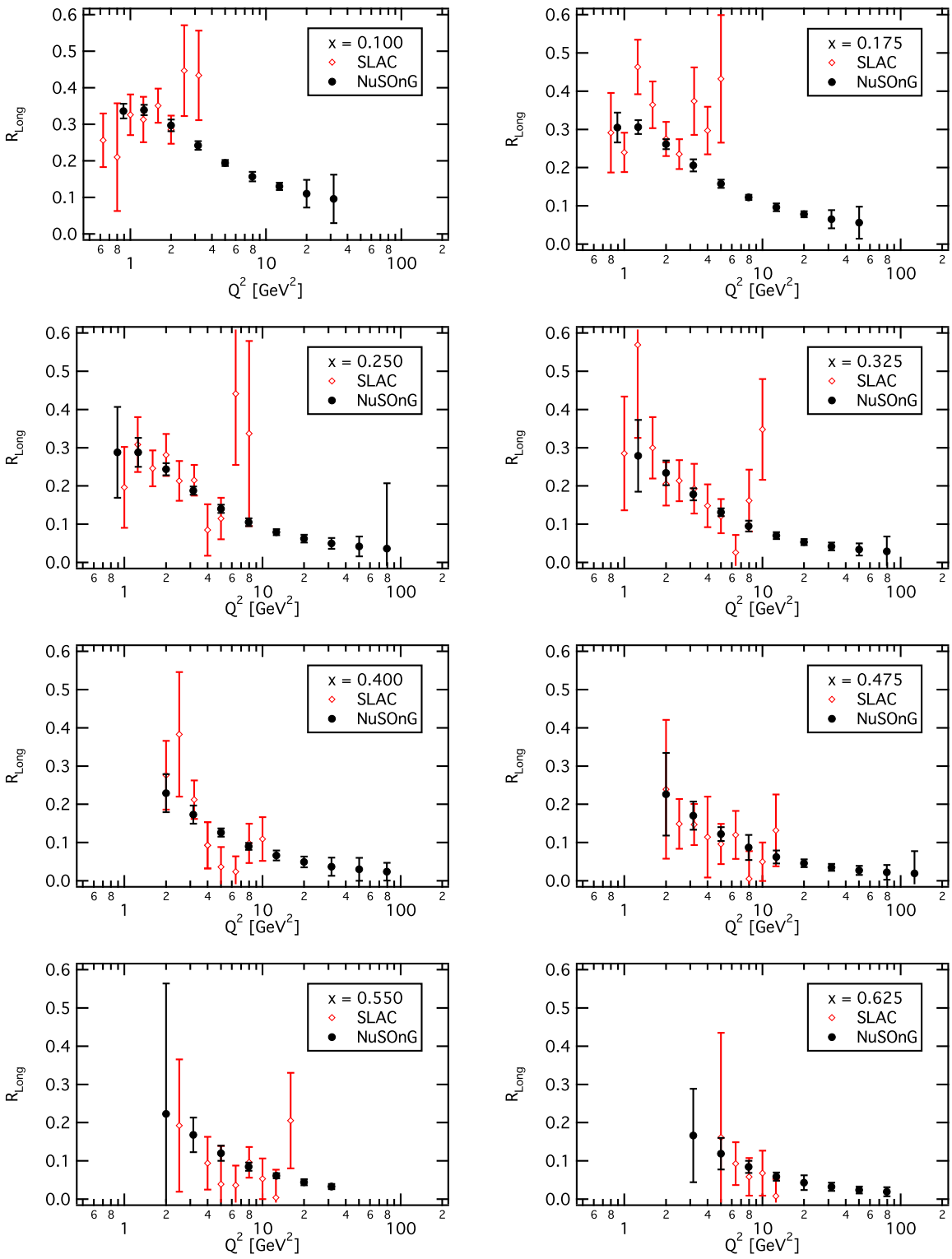

Figure 7: Extracted values of R (labeled NuSOnG) from the four structure function fits as compared to previous measurements[16] (labeled SLAC).

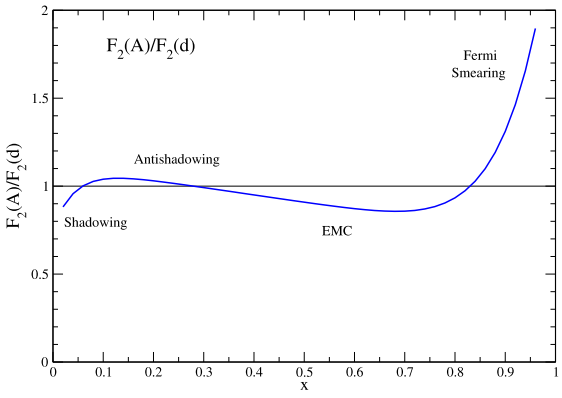

Figure 8: Typical behavior of the ratio of the structure function on a nuclear target A to that on a deuterium target.

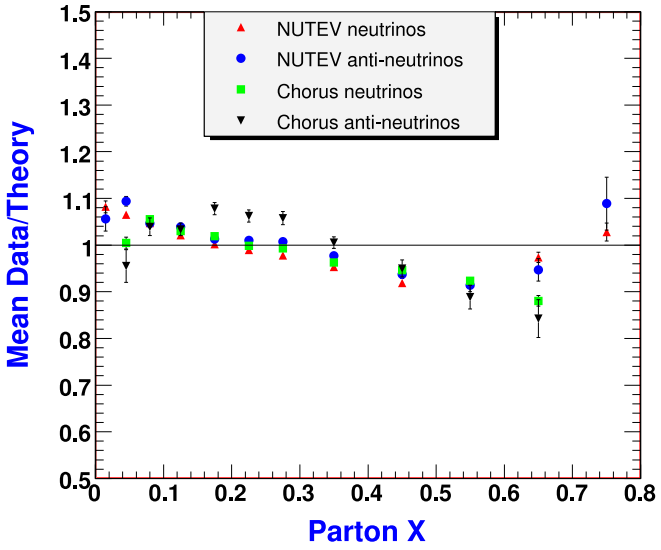

Figure 9: Comparison between the reference fit and the unshifted CHORUS and NuTeV neutrino data without any nuclear corrections.

C. Measuring Nuclear Effects with the Minerva and NuSOnG Detectors

The Minerva experiment will also be studying neutrino induced nuclear effects and will be starting its initial physics run in early 2010. To study nuclear effects in Minerva, a cryogenic vessel containing liquid helium (0.2 ton fiducial mass)will be installed upstream of the Minerva detector. Within the Minerva detector, solid carbon, iron and lead targets will be installed upstream of the pure scintillator active detector. The total mass is 0.7 ton of Fe, 0.85 ton of Pb, 0.4 ton of He and somewhat over 0.15 ton of C. Since the pure scintillator active detector essentially acts as an additional 3-5 ton carbon target (CH), the pure graphite (C) target is mainly to check for consistency. For a run consisting of 4.0 x 10^{20} POT in the NuMI Low Energy (LE) beam and 12×10^{20} POT in the NuMI Medium Energy (ME) beam, Minerva would collect over 2 M events on Fe, 2.5 M events on Pb, 600 K on helium and 430 K events on C as well as 9.0 M events on the scintillator within the fiducial volume.

Material	Mass of 2.54 cm slab (tons)	Number of slabs needed for NuTeV-equivalent statistics
C	1.6	33
Al	1.9	27
Fe	5.5	10
Pb	7.9	7

Table II: Alternative target materials for cross-section analysis

Studying nuclear effects with the NuSOnG detector will involve fewer nuclear targets but considerably more statistics on each. In addition, the much higher energy of the incoming neutrinos with NuSOnG means a much wider kinematic range of study. In particular, NuSOnG will have a much higher Q^2 for a given low-x to study shadowing by neutrinos and will be able to measure the shadowing region down to much smaller x for the same Q^2 range as Minerva. A significant addition to the study of nuclear effects with neutrinos would be the addition of a large, perhaps active ("Bubble Chamber"), cryogenic target containing hydrogen or deuterium. With the intense NuSOnG neutrino beam, a significant sample of neutrino-hydrogen and neutrino-deuterium events could provide the normalization we need to further unfold nuclear effects in neutrino-nucleus interactions.

V. QCD FITS

The extraction of up to six structure functions from the cross sections of neutrino and anti-neutrino DIS discussed so far (*cf*, Eq. (1)) has been completely model-independent relying only on some fundamental principles such as Lorentz-invariance of the cross section and gauge-invariance of the hadronic tensor which is expanded in terms of the structure functions which parameterize the unknown hadronic physics.

More can be said about the structure functions in QCD. While it is still not possible to accurately compute the x-dependence of the structure functions from first principles, QCD allows us to derive renormalization group equations (RGEs) which relate the structure functions at different (perturbative) scales Q. Note that the structure functions at the scale Q can be directly related to structure functions at a different scale Q_0 (see, e.g., Eqs. (5.58) and (5.76) in [31]). However, it is more convenient to work in the QCD-improved parton model where the RGEs governing the scale-dependence of the parton distribution functions (PDFs) are the familiar DGLAP evolution equations; these can also be used to compute the structure functions at Q given the PDFs at that scale.

[32, 33, 34] Furthermore, this approach has the crucial advantage that the universal PDFs allow us to make predictions for other observables as well. In addition to the Q-dependence, the QCD calculations provide certain (approximate) relations between different structure functions as will be visible from the parton model expressions below.

In this section we will discuss the analysis of the cross section data within the framework of the QCD-improved parton model. Already in the past, high statistics measurements of neutrino deeply inelastic scattering (DIS) on heavy nuclear targets (NuTeV, ...) have attracted much interest in the literature since they provide valuable information for global fits of PDFs [35, 36].

Due to the weak nature of neutrino interactions, the use of nuclear targets is unavoidable; this complicates the extraction of free nucleon PDFs, because model-dependent corrections must be applied to the data (*cf* Sec. IV). Of course, these same data are also useful for extracting the *nuclear* parton distribution functions (NPDFs) and for such an analysis no nuclear correction factors are required. Conversely, the NPDFs can be utilized to compute the required nuclear correction factors within the QCD parton model [37]. Similar to proton PDFs, universal nuclear PDFs are needed for the description of many processes with nuclei in the initial state. This involves physics at other neutrino experiments, heavy ion colliders (RHIC, LHC), and a possible future electron-ion collider (EIC).

The NuSOnG experiment will have two orders of magnitude higher statistics than the NuTeV and CCFR experiments (over an extended kinematic range), and so it will be possible to study small effects such as the strangeness asymmetry with better precision, or to establish for the first time isospin violation in the light quark sector. Better understanding these effects is relevant for improving the extraction of the weak mixing angle in a Paschos–Wolfenstein type analysis.

A. PDFs

NuSOnG will perform measurements on different nuclear targets. The PDFs for a nucleus (A, Z) are constructed as

$$f_i^A(x,Q) = \frac{Z}{A}\, f_i^{p/A}(x,Q) + \frac{(A-Z)}{A}\, f_i^{n/A}(x,Q)\,. \quad (13)$$

In the following discussion we take into account deviations from isospin symmetry, a non-vanishing strangeness asymmetry and the possibility to have non-isoscalar targets. For this purpose we introduce the following linear combinations of strange quark PDFs:

$$s^{+,A} = s^A + \bar{s}^A\,, \quad s^{-,A} = s^A - \bar{s}^A\,, \quad (14)$$

where the strangeness asymmetry is described by a non-vanishing PDF s^-. Note however that we continue to assume $s^{p/A} = s^{n/A}$ and $\bar{s}^{p/A} = \bar{s}^{n/A}$. Also, we neglect any possible charm asymmetry, i.e., we use $c^A = \bar{c}^A$ such that $c^{-,A} = c^A - \bar{c}^A = 0$ and $c^{+,A} = c^A + \bar{c}^A = 2c^A$.

Deviations from isospin symmetry can be parameterized in the following way:

$$\delta u_v^{p/A} = u_v^{p/A} - d_v^{n/A}\,,\ \delta d_v^{p/A} = d_v^{p/A} - u_v^{n/A}\,, \quad (15)$$

$$\delta \bar{u}^{p/A} = \bar{u}^{p/A} - \bar{d}^{n/A}\,,\ \delta \bar{d}^{p/A} = \bar{d}^{p/A} - \bar{u}^{n/A}\,. \quad (16)$$

These definitions allow us to write the PDFs in a way which makes deviations from isoscalarity and isospin symmetry manifest:

$$2u_v^A = [u_v^{p/A} + d_v^{p/A} - \delta d_v^{p/A}] - \Delta[u_v^{p/A} - d_v^{p/A} + \delta d_v^{p/A}]\,, \quad (17)$$

$$2d_v^A = [u_v^{p/A} + d_v^{p/A} - \delta u_v^{p/A}] + \Delta[u_v^{p/A} - d_v^{p/A} - \delta u_v^{p/A}]\,, \quad (18)$$

$$2\bar{u}^A = [\bar{u}^{p/A} + \bar{d}^{p/A} - \delta \bar{d}^{p/A}] - \Delta[\bar{u}^{p/A} - \bar{d}^{p/A} + \delta \bar{d}^{p/A}]\,, \quad (19)$$

$$2\bar{d}^A = [\bar{u}^{p/A} + \bar{d}^{p/A} - \delta \bar{u}^{p/A}] + \Delta[\bar{u}^{p/A} - \bar{d}^{p/A} - \delta \bar{u}^{p/A}]\,, \quad (20)$$

where $\Delta = (N-Z)/A$ parameterizes the deviation from isoscalarity. We have written Eqs.(17)–(20) so that the RHS is expressed explicitly in terms of proton PDFs and the four δ-terms $\{\delta u_v^{p/A}, \delta d_v^{p/A}, \delta \bar{u}^{p/A}, \delta \bar{d}^{p/A}\}$; the δ-terms vanish individually if isospin symmetry is preserved.

B. Structure functions

The structure functions for a nuclear target (A, Z) are given by

$$F_i^A(x,Q) = \frac{Z}{A}\, F_i^{p/A}(x,Q) + \frac{(A-Z)}{A}\, F_i^{n/A}(x,Q) \quad (21)$$

such that they can be computed in next-to-leading order as convolutions of the nuclear PDFs with the conventional Wilson coefficients, *i.e.*, generically

$$F_i^A(x,Q) = \sum_k C_{ik} \otimes f_k^A\,. \quad (22)$$

In order to discuss which information can be extracted from a high statistics measurement of neutrino and antineutrino DIS cross sections we briefly review the parton model expressions for the 6 structure functions. For simplicity, we first restrict ourselves to leading order, neglect heavy quark mass effects (as well as the associated production thresholds), and assume a diagonal CKM matrix. In our numerical results, these effects are taken into account.

The neutrino–nucleus structure functions are given by (suppressing the dependence on x and Q^2):

$$F_1^{\nu A} = d^A + s^A + \bar{u}^A + \bar{c}^A + \ldots\,, \quad (23)$$

$$F_2^{\nu A} = 2xF_1^{\nu A}\,, \quad (24)$$

$$F_3^{\nu A} = 2\left[d^A + s^A - \bar{u}^A - \bar{c}^A + \ldots\right]\,. \quad (25)$$

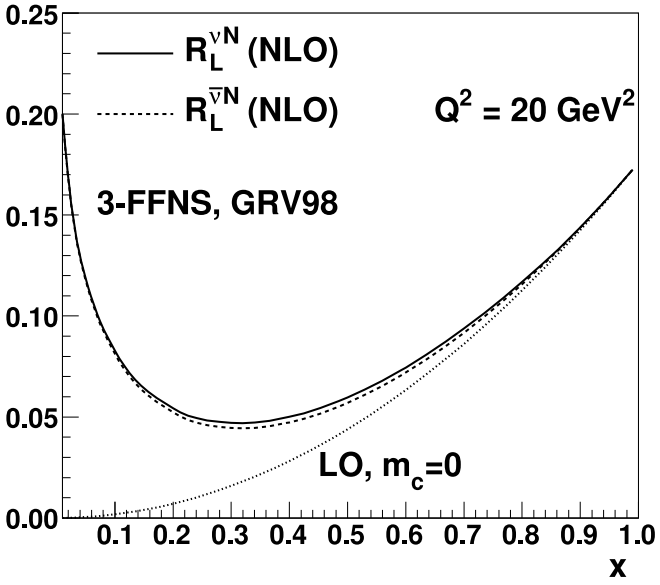

Figure 10: Structure function ratio R_L for neutrino and anti-neutrino nucleon ($N = (p+n)/2$)) scattering at $Q^2 = 20$ GeV^2. The solid and dashed lines show NLO results obtained with the GRV98 PDFs [38], while the dotted line shows the LO result of Eq. (31).

The structure functions for anti-neutrino scattering are obtained by exchanging the quark and anti-quark PDFs in the corresponding neutrino structure functions:

$$F_{1,2}^{\bar\nu A} = F_{1,2}^{\nu A}[q \leftrightarrow \bar q] \,, \qquad F_3^{\bar\nu A} = -F_3^{\nu A}[q \leftrightarrow \bar q] \,. \quad (26)$$

Explicitly this gives

$$F_1^{\bar\nu A} = u^A + c^A + \bar d^A + \bar s^A + \ldots \,, \quad (27)$$
$$F_2^{\bar\nu A} = 2x F_1^{\bar\nu A} \,, \quad (28)$$
$$F_3^{\bar\nu A} = 2\left[u^A + c^A - \bar d^A - \bar s^A + \ldots\right] . \quad (29)$$

The longitudinal structure function can be obtained with the help of the following relation:

$$F_L^{\nu A} = r^2 F_2^{\nu A} - 2x F_1^{\nu A} = \frac{4x^2M^2}{Q^2} F_2^{\nu A} \,, \quad (30)$$

where $r^2 = 1 + 4x^2M^2/Q^2$. Finally, it is customary to introduce the ratio of longitudinal to transverse structure functions:

$$R_L^{\nu A} = \frac{F_L^{\nu A}}{2x F_1^{\nu A}} = \frac{r^2 F_2^{\nu A}}{2x F_1^{\nu A}} - 1 = \frac{4x^2M^2}{Q^2} \,. \quad (31)$$

Similar equations hold for anti-neutrino scattering. As can be seen, in leading order $R_L^\nu = R_L^{\bar\nu}$. As is shown in Fig. 10, also in NLO, the differences between R_L^ν and $R_L^{\bar\nu}$ are tiny such that the difference between these two functions can be neglected in the following discussion.

C. Constraints on the PDFs

The differential cross section in Eq. (1) can be written as:

$$\frac{d\sigma}{dxdy} = K[A + B(1-y)^2 + Cy^2] \quad (32)$$

with $K = \frac{G_F^2 ME}{2\pi(1+Q^2/M_W^2)^2}$, $A = F_2 \pm xF_3$, $B = F_2 \mp xF_3$, and $C = \frac{2x^2M^2}{Q^2}F_2 - F_L$ where the upper sign refers to neutrino and the lower one to anti-neutrino scattering. This form of $d\sigma$ shows that the (anti-)neutrino cross section data naturally encodes information on the four structure function combinations $F_2^{\nu A} \pm xF_3^{\nu A}$ and $F_2^{\bar\nu A} \pm xF_3^{\bar\nu A}$ in separate regions of the phase space. In addition, at large y the structure function combination C contributes. However, to good accuracy $C^\nu = C^{\bar\nu}$ so that C drops out in the difference of neutrino and anti-neutrino cross sections.

Assuming $s^A = \bar s^A$ and $c^A = \bar c^A$, the structure functions $F_2^{\nu A}$ and $F_2^{\bar\nu A}$ constrain the valence distributions $d_v^A = d^A - \bar d^A$, $u_v^A = u^A - \bar u^A$ and the flavor-symmetric sea $\Sigma^A := \bar u^A + \bar d^A + \bar s^A + \bar c^A + \ldots$ via the relations:

$$\frac{1}{x}F_2^{\nu A} = 2\left[d_v^A + \Sigma^A\right] , \quad (33)$$
$$\frac{1}{x}F_2^{\bar\nu A} = 2\left[u_v^A + \Sigma^A\right] . \quad (34)$$

Furthermore, we have

$$\frac{1}{x}F_2^{\nu A} + F_3^{\nu A} = 4(d^A + s^A) \,, \quad (35)$$
$$\frac{1}{x}F_2^{\bar\nu A} - F_3^{\bar\nu A} = 4(\bar d^A + \bar s^A) \,. \quad (36)$$

Since we constrain the strange distribution utilizing the dimuon data, the latter two structure functions are useful to separately extract the d^A and $\bar d^A$ distributions.

For an isoscalar nucleus we encounter further simplifications. In this case, $u^A = d^A$ and $\bar u^A = \bar d^A =: \bar q^A$ which implies $u_v^A = d_v^A =: v^A$. Hence, the independent quark distributions are $\{v^A, \bar q^A, s^A = \bar s^A, c^A = \bar c^A, \ldots\}$. In particular, we have $F_2^{\nu A} = F_2^{\bar\nu A}$ for an isoscalar target such that our original set of 6 independent structure functions reduces to 3 independent functions (say $F_2^{\nu A}$, $F_3^{\nu A}$, $F_3^{\bar\nu A}$) under the approximations made.

In a more refined analysis, allowing for a non-vanishing strangeness asymmetry and isospin violation we can evaluate the non-singlet structure function $\Delta F_2^\nu \equiv F_2^{\nu A} - F_2^{\bar\nu A}$ with the help of the relations in Eqs. (17) – (20):

$$\Delta F_2^\nu = 2xs^{-,A} + x\,\delta d_v^{p/A} - x\,\delta u_v^{p/A} + \Delta x[2u_v^{p/A} - 2d_v^{p/A} + \delta d_v^{p/A} - \delta u_v^{p/A}] \,. \quad (37)$$

For a nuclear isoscalar target ($Z = N = A/2$, $\Delta = 0$) this expression simplifies to

$$\Delta F_2^\nu = 2xs^{-,A} + x\,\delta d_v^{p/A} - x\,\delta u_v^{p/A} \,. \quad (38)$$

As one can see, ΔF_2^ν will be small and sensitive to the strangeness asymmetry and isospin violating terms for the valence quarks.

The difference of the neutrino and anti-neutrino cross-sections provides, in principle, access to this quantity:

$$\frac{d^2\sigma^{\nu A}}{dxdy} - \frac{d^2\sigma^{\bar\nu A}}{dxdy} \simeq K[\Delta F_2^\nu + xF_3^\nu + (1-y)^2(\Delta F_2^\nu - xF_3^\nu)] \quad (39)$$

with $F_3^\nu = F_3^{\nu A} + F_3^{\bar\nu A}$.

It should be noted, however, that in a global fit to extract structure functions we do not make direct use of these equations [the $(1-y)^2$-dependence] but simply perform a χ^2-analysis of all neutrino and anti-neutrino cross section data.

VI. ISOSPIN (CHARGE SYMMETRY) VIOLATION AND ΔxF_3

The question of isospin violation is central to the PW electroweak measurement. In the NuTeV analysis, isospin symmetry was assumed. As discussed in Ref. [3], various models which admit isospin violation can pull the NuTeV $\sin\theta_W$ measurement toward the Standard Model. However it would take significantly larger isospin violation to bring NuTeV into agreement with the rest of the world's data. Better constraints of isospin violation will be crucial to the interpretation of the NuSOnG results.

When we relate DIS measurements from heavy targets such as $^{56}_{26}$Fe (used in NuTeV) or $^{207}_{82}$Pb (Chorus) back to a proton or isoscalar target, we generally make use of isospin symmetry where we assume that the proton and neutron PDFs can be related via a $u \leftrightarrow d$ interchange. While isospin symmetry is elegant and well motivated, the validity of this exact charge symmetry must ultimately be established by experimental measurement. There have been a number of studies investigating isospin symmetry violation [39, 40, 41, 42, 43, 44, 45]; therefore, it is important to be aware of the magnitude of potential violations of isospin symmetry and the consequences on the extracted PDF components. For example, the naive parton model relations are modified if we have a violation of exact $p \leftrightarrow n$ isospin-symmetry, or charge symmetry violation (CSV); *e.g.*, $u^n(x) \not\equiv d^p(x)$ and $u^p(x) \not\equiv d^n(x)$.

It is noteworthy that a violation of isospin symmetry is automatically generated once QED effects are taken into account [46, 47, 48]. This is because the photon couples to the up quark distribution $u^p(x)$ differently than to the down quark distribution $d^n(x)$. These terms can be as much as a few percent in the medium x range, see *e.g.* Fig. 1 in Ref. [48].

Combinations of structure functions can be particularly sensitive to isospin violations, and NuSOnG is well suited to measure some of these observables. For example, residual u,d-contributions to $\Delta xF_3 = xF_3^\nu - xF_3^{\bar\nu}$ from charge symmetry violation would be amplified due to enhanced valence components $\{u_v(x), d_v(x)\}$, and because the $d \to u$ transitions are not subject to slow-rescaling corrections which suppress the $s \to c$ contribution to ΔxF_3 [41]. Here the ability of NuSOnG to separately measure xF_3^ν and $xF_3^{\bar\nu}$ over a broad kinematic range will provide powerful constraints on the sensitive structure function combination ΔxF_3.

Separately, the measurement of $\Delta F_2 \equiv \frac{5}{18}F_2^{CC}(x,Q^2) - F_2^{NC}(x,Q^2)$ in Charged Current (CC) $W^\pm$ exchange and Neutral Current (NC) γ/Z exchange processes can also constrain CSV [43]; because NuSOnG will measure F_2^{CC} on a variety of targets, this will reduce the systematics associated with the heavy nuclear target corrections thus providing an additional avenue to study CSV.

In the following, we provide a detailed analysis of CSV which also investigates the various experimental systematics associated with each measurement. We shall find it is important to consider all the systematics which impact the various experimental measurements to assess the discriminating power.

A. ΔxF_3 and Isospin Violations

We recall the leading-order relations of the neutrino structure function F_3 on a general nuclear target:

$$\frac{1}{2}F_3^{\nu A}(x) = d^A + s^A - \bar u^A - \bar c^A + ..., \quad (40)$$

$$\frac{1}{2}F_3^{\bar\nu A}(x) = u^A + c^A - \bar d^A - \bar s^A + ... \quad (41)$$

where A represents the nuclear target $A = \{p, n, d, ...\}$, and the "..." represent higher-order contributions and terms from the third generation $\{b, t\}$ quarks. Note that to illustrate the general features of these processes, we use a schematic notation as in Eq. (40) and Eq. (41); for the numerical calculations, the full NLO expressions are employed including mass thresholds, "slow-rescaling" variables, target mass corrections, and CKM elements where appropriate.

For a nuclear target A we can construct ΔxF_3^A as:

$$\begin{aligned}\Delta xF_3^A &= xF_3^{\nu A} - xF_3^{\bar\nu A} \\ &= 2x\Delta\left[\left(u^{p/A} - d^{p/A}\right) + \left(\bar u^{p/A} - \bar d^{p/A}\right) + \frac{1}{2}\delta I^A\right] \\ &+ 2x\, s^{+,A} - 2xc^{+,A} + x\,\delta I^A + \mathcal{O}(\alpha_S) \end{aligned} \quad (42)$$

where $\mathcal{O}(\alpha_S)$ represents the higher order QCD corrections, and the isospin violations are given by δI^A:

$$\delta I^A = \delta d - \delta u + \delta\bar d - \delta\bar u\,. \quad (43)$$

For a flux-weighted linear combination of F_3^ν and $F_3^{\bar\nu}$, terms proportional to the strange quark asymmetry can enter Eq. (42), *cf.* Refs. [39, 43, 44]. For a sign-selected $\nu/\bar\nu$ beam as for NuTeV or NuSOnG, this complication is

not necessary. We have defined $s^{\pm,A}(x) = [s^A(x) \pm \bar{s}^A(x)]$ and $c^{\pm,A}(x) = [c^A(x) \pm \bar{c}^A(x)]$.

In the limit of isospin symmetry, all four terms on the RHS of Eq. (43) vanish individually. For a nuclear isoscalar target, $Z = N = A/2$, we can construct $\Delta x F_3$ from the above:

$$\Delta x F_3 = x F_3^{\nu A} - x F_3^{\bar{\nu} A} = 2x s^{+,A} - 2x c^{+,A} + x\,\delta I^A + \mathcal{O}(\alpha_S) \ . \quad (44)$$

Note in Eq. (42) that for a nuclear target A which is close to isoscalar we have $Z \sim N$ such that the up and down quark terms are suppressed; this is a benefit of the NuSOnG glass (SiO_2) target which is very nearly isoscalar. More specifically, for SiO_2 we have $Z(\mathrm{O}) = 8$, $Z(\mathrm{Si}) = 14$, $m(\mathrm{O}) = 15.994$, $m(\mathrm{Si}) = 28.0855$. Using $A = Z + N$ we have $(N-Z)/A = (A-2Z)/A$ for the prefactor in Eq. (42) which yields $(N-Z)/A \sim -0.000375$ for O and $(N-Z)/A \sim 0.00304$ for Si.

In Eq. (42) the PDFs $\{u^{p/A}, d^{p/A}, ...\}$ represent quark distributions bound in a nucleus A. With a single nuclear target, we can determine the CSV term δI^A for this specific A; measurements on different nuclear targets would be required in order to obtain the A dependence of δI^A if we need to scale to a proton or isoscalar target.

Thus, an extraction of any isospin violation δI^A requires a careful separation of these contributions from the strange, charm, and higher order terms. Theoretical NLO calculations for $\Delta x F_3$ are available; thus the $\mathcal{O}(\alpha_S)$ corrections can be addressed. Additionally, NuSOnG can use the dimuon process ($\nu N \to \mu^+\mu^- X$) to constrain the strange sea.

In conclusion we find that while this is a challenging measurement, NuSOnG's high statistics measurement of $\Delta x F_3$ should provide a window on CSV which is relatively free of large experimental systematics. We emphasize that $\Delta x F_3$ may be extracted from a single target, thereby avoiding the complications of introducing nuclear corrections associated with different targets. This is in contrast to the other measurements discussed below. However, if we desire to rescale the δI^A effects to a different nucleus A, then multiple targets would be required.

B. Measurement of $\Delta F_2 \equiv \frac{5}{18} F_2^{CC}(x,Q^2) - F_2^{NC}(x,Q^2)$

A separate determination of CSV can be achieved using the measurement of F_2 in CC and NC processes via the relation:

$$\begin{aligned} \Delta F_2 \ &\equiv \ \frac{5}{18} F_2^{CC,A}(x,Q^2) - F_2^{NC,A}(x,Q^2) \\ &\simeq \ \frac{1}{6} x \frac{(N-Z)}{A} \left[\left(u^{p/A} - d^{p/A} \right) + \left(\bar{u}^{p/A} - \bar{d}^{p/A} \right) \right] \\ &+ \ \frac{1}{6} x\, s^{+,A}(x) - \frac{1}{6} x\, c^{+,A}(x) + \frac{1}{6} x \frac{N}{A} \delta I^A \\ &+ \ \mathcal{O}(\alpha_s) \end{aligned} \quad (45)$$

with the definitions:

$$F_2^{CC,A} = \frac{1}{2} \left[F_2^{\nu A} + F_2^{\bar{\nu} A} \right]$$

$$F_2^{NC,A} = F_2^{\ell A}$$

In Eq. (45), the first term is proportional to $(N-Z)/A$ which vanishes for an isoscalar target. The second and third terms are proportional to the heavy quark distributions $s^{+,A}$ and $c^{+,A}$. The next term is the CSV contribution which is proportional to δI^A given in Eq. (43). It is curious that this has the same form as the CSV contribution for $\Delta x F_3$ of Eq. (42). Finally, the last term represents the higher-order QCD corrections.

While the character of the terms on the LHS of Eq. (44) and Eq. (45) are quite similar, the systematics of measuring ΔF_2 may differ substantially from that of $\Delta x F_3$. For example, the measurement of ΔF_2 requires the subtraction of structure functions from two entirely different experiments. The CC neutrino–nucleon data are extracted from heavy nuclear targets (to accumulate sufficient statistics); as such, these data are generally subject to large nuclear corrections so that the heavy targets can be related to the isoscalar $N = \frac{1}{2}(p+n)$ limit. Conversely, the NC charged-lepton–nucleon process proceeds via the electromagnetic interaction. Therefore sufficient statistics can be obtained for light targets including H and D and no large heavy target corrections are necessary. Therefore, we must use the appropriate nuclear correction factors when we combine F_2^{CC} and F_2^{NC}, and this will introduce a systematic uncertainty.

Separately, the heavy quark production mechanism is different in the CC and NC processes. Specifically, in the CC case we encounter the process $s + W^+ \to c$ where the charm mass threshold kinematics must be implemented. On the other hand, the NC process is $c + \gamma \to c$ which is proportional to the charm sea distribution and has different threshold behavior than the CC process. Even though the charm production process is modeled at NLO, the theoretical uncertainties which this introduces can dominate precision measurements.

C. Other Measurements of CSV

We very briefly survey other measurements of CSV in comparison to the above.

The measurement of the lepton charge asymmetry in W decays from the Tevatron can constrain the up and down quark distributions [49, 50]. In this case, the extraction of CSV constraints is subtle; while isospin symmetry is not needed to relate p and $\bar{p}$, this symmetry is typically used in a global fit of the PDFs to reduce data on heavy targets to p.

In the limit that all the data in the analysis were from proton targets, CSV would not enter; hence this limit only arises indirectly from the mix of targets which enter

a global fit. At present, while much of the data does come from proton targets (H1, ZEUS, CDF, D0), there are some data sets from both p and d (BCDMS, NMC, E866), and some that use heavier targets (E-605, NuTeV) [29, 51]. Thus, an outstanding question is if CSV were present, to what extent would this be "absorbed" into a global fit. The ideal procedure would be to parameterize the CSV and include this in a global analysis. While this step has yet to be implemented, there is a recent effort to include the nuclear corrections as a dynamic part of a global fit [37].

Additionally, NMC measures F_2^n/F_2^p data which has an uncertainty of order a few percent [52]. There are also fixed-target Drell-Yan experiments such as NA51 [45] and E866 [53] which are sensitive to the ratio $\bar{d}/\bar{u}$ in the range $0.04 < x < 0.27$. We will soon have LHC data (pp) to add to our collection, thus providing additional constraints in a new kinematic region.

D. Conclusions on Charge Symmetry Violation

NuSOnG will be able to provide high statistics DIS measurements across a wide x range. Because the target material (SiO_2) is nearly isoscalar, this will essentially allow a direct extraction of the isoscalar observables.

ΔxF_3 is one of the cleaner measurements of CSV in terms of associated experimental systematic uncertainties as this measurement can be extracted from a single target. The challenge here will be to maximize the event samples.

The measurement of ΔF_2 is more complicated as this must combine measurements from both CC and NC experiments which introduces nuclear correction factors [37, 54]. Since NuSOnG will provide high statistics F_2^{CC}measurements for a variety of A targets, this will yield an alternate handle on the CSV and also improve our understanding of the associated nuclear corrections.

The combination of these measurements, together with external constraints, will yield important information on this fundamental symmetry.

VII. MEASUREMENTS OF THE HEAVY QUARKS

A. Measurement of the Strange Sea

Charged current neutrino-induced charm production, $(\nu/\bar{\nu})N \to \mu^+\mu^- X$, proceeds primarily through the subprocesses $W^+ s \to c$ and $W^- \bar{s} \to \bar{c}$ (respectively), so this provides a unique mechanism to directly probe the $s(x)$ and $\bar{s}(x)$ distributions. Approximately 10% of the time the charmed particles decay into $\mu + X$, adding a second oppositely signed muon to the CC event's final state. These "dimuon" events are easily distinguishable, and make up approximately 1% of the total CC event sample. Hence, the recent high statistics dimuon measurements [17, 18, 55, 56, 57] play an essential role in constraining the strange and anti-strange components of the proton. On NuSOnG, the dimuon data will be used in the same manner.

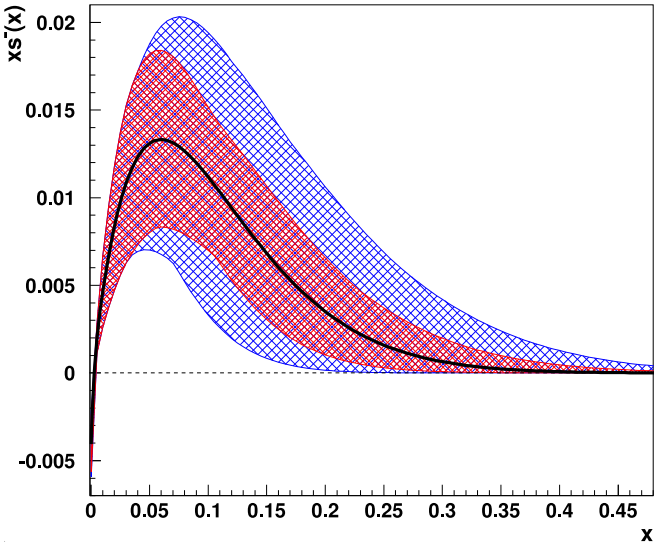

Figure 11: NuTeV measurement of $xs^-(x)$ vs x at $Q^2 = 16\,\mathrm{GeV}^2$. Outer band is combined errors, inner band is without B_c uncertainty.

Distinguishing the difference between the $s(x)$ and $\bar{s}(x)$ distributions,

$$xs^-(x) \equiv xs(x) - x\bar{s}(x), \tag{46}$$

is necessary for the PW style analysis. This analysis is sensitive to the integrated strange sea asymmetry,

$$S^- \equiv \int_0^1 s^-(x)dx, \tag{47}$$

through its effect on the denominator of the PW ratio, as has been recognized in numerous references [58, 59, 60, 61, 62]).

The highest precision study of s^- to date is from the NuTeV experiment [55, 63]. The sign selected beam allowed measurement of the strange and anti-strange seas independently, recording 5163 neutrino-induced dimuons, and 1380 antineutrino induced dimuon events in its iron target. Figure 11 shows the fit for asymmetry between the strange and anti-strange seas in the NuTeV data.

The integrated strange sea asymmetry from NuTeV has a positive central value: 0.00196 ± 0.00046 (stat) ± 0.00045 (syst) $^{+0.00148}_{-0.00107}$ (external). In NuSOnG, as in NuTeV, the statistical error will be dominated by the antineutrino data set and is expected to be about 0.0002. The systematic error is dominated by the π and K decay-in-flight subtraction. This can be addressed in NuSOnG through test-beam measurements which will allow a more accurate modeling of this background, as well as applying

the techniques of CCFR to constrain this rate [64, 65, 66]. We expect to be able to reduce this error to about 0.0002. The combination of these reduces the total error by about 10%, because the main contributon comes from the external inputs.

The external error on the measurement is dominated by the error on the average charm semi-muonic branching ratio, B_c:

$$B_c = \Sigma_i \int \phi(E) f_i(E) B_{\mu - i} dE, \qquad (48)$$

where ϕ is the neutrino flux in energy bins, f_i is the energy dependent production fraction for each hadron, and $B_{\mu-i}$ is the semi-muonic branching ratio for each hadron. In the NuTeV analysis, this is an external input, with an error of about 10%. To make further progress, this error must be reduced.

Fig. 12 shows the world measurements of B_c, taken from references [17, 56, 57, 67, 68, 69, 70]. Measuring B_c directly requires the capability to resolve the individual charmed particles created in the interaction. The best direct measurements are from emulsion. This kind of measurement has been performed in past experiments (E531, Chorus) using emulsion detectors [69, 70], where the decay of the charmed meson is well tagged. Since the cross section for charmed meson production is energy dependent, it is important to make a measurement near the energy range of interest. The NuTeV strange sea asymmetry study used a re-analysis of 125 charm events measured by the FNAL E531 experiment [69] in the energy range of the NuTeV analysis ($E_\nu > 20$ GeV). B_c has also been constrained through indirect measurement via fits.

For NuSOnG, our goal is to reduce the error on B_c using an *in situ* measurement on glass by at least a factor of 1.5. One method is to include B_c as a fit parameter in the analysis of the dimuon data. The unprecedentedly high statistics will allow a fit as a function of neutrino energy for the first time. Dimuons from high x neutrino DIS almost exclusively result from scattering off valence quarks, such that the dimuon cross section in that region isolates B_c from the strange sea. In dimuon fits, the assumption is then taken that $B_{c-\nu} = B_{c-\overline{\nu}}$, B_c may be measured directly from the dimuon data.

Unfortunately, antineutrino charm production is not well measured by past experiments. This leads to concerns about the assumption that $B_{c-\nu} = B_{c-\overline{\nu}}$. An example of a potential source of difference in neutrino and antineutrino mode, consider that $\nu n \to \mu^- \Lambda_c$ has no analogous reaction in the antineutrino channel.

These arguments provide the motivation for including a high resolution target/tracker in the NuSOnG design that can directly measure the semileptonic branching ratio to charm in both ν and $\bar{\nu}$ running modes. There are two feasible detector technologies. The first is to use emulsion, as in past experiments. This is proven technology and scanning could be done at the facility in Nagoya, Japan. The second is to use the NOMAD-STAR detector

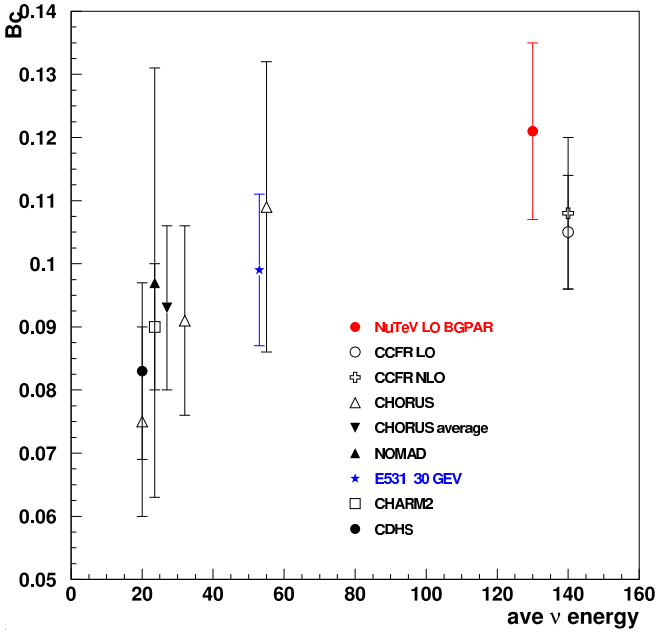

Figure 12: World measurements of B_c. See refs. [17, 56, 57, 67, 68, 69, 70].

[71, 72] or a similar detector. This is a 45 kg silicon vertex detector which ran in front of the NOMAD experiment. The target was boron carbide interleaved with the silicon. This detector successfully measured 45 charm events in that beam, identifying D^+, D^0 and D_s. A similar detector of this size in the NuSOnG beam would yield about 900 ν events and 300 $\bar{\nu}$ events. This has the advantage of being a low-Z material which is isoscalar and close in mass to the SiO_2 of the detector.

B. Strange Quark Contribution to the Proton Spin

An investigation of the strange quark contribution to the elastic vector and axial form factors of the proton is possible in NuSOnG, by observing NC elastic and CC quasi-elastic scattering events; namely $\nu p \to \nu p$ and $\nu n \to \mu^- p$ events in neutrino mode, and $\bar{\nu} p \to \bar{\nu} p$ and $\bar{\nu} p \to \mu^+ n$ events in antineutrino mode. The motivation for making this measurement comes from a number of recent (and not so recent) studies in proton structure.

Over the last 15 years a tremendous effort has been made at MIT-Bates, Jefferson Lab, and Mainz to measure the strange quark contribution to the vector form factors (that is, the electromagnetic form factors) of the proton via parity-violating electron scattering from protons, deuterons, and ^{4}He [73, 74, 75, 76, 77, 78, 79, 80, 81, 82, 83]. The technique is to observe the parity-violating beam spin asymmetry in elastic scattering of longitudinally polarized electrons from these unpolarized targets; this asymmetry is caused by an interference between the one-photon and one-Z exchange amplitudes [84]. As a result, the weak neutral current analog of the electro-

magnetic form factors of the proton may be measured and this gives access to the strange quark contribution. This worldwide experimental program will soon be complete. The results available to date (from global analyses [85, 86, 87]) indicate a small (and nearly zero) contribution of the strange quarks to the elastic electric form factor, G_E^s; this is not surprising, as the total electric charge in the proton due to strange quarks is zero. At the same time, these same data point to a small but likely positive contribution of the strange quarks to the elastic magnetic form factor, G_M^s, indicating a small positive contribution of the strange quarks to the proton magnetic moment. Due to the prominent role played by the Z-exchange amplitude, these experiments are also sensitive to the strange quark contribution to the elastic *axial* form factor, which is related to the proton spin structure.

It is now well established by leptonic deep inelastic scattering experiments that the spins of the valence and sea quarks in the proton together contribute about 30% of the total proton intrinsic angular momentum of $\hbar/2$. The strange quark contribution is estimated to be about -10% in inclusive DIS (an analysis which makes use of SU(3)-flavor symmetry) [88], but is found to be approximately zero in semi-inclusive DIS (an alternative analysis which makes no use of SU(3) but needs fragmentation functions instead) [89]. A recent global analysis [90] which made use of both inclusive and semi-inclusive DIS and which allowed for the possibility of SU(3)-flavor violation found no need in the data for any violation of SU(3) and indicated a small negative contribution of strange quarks to the proton spin. In the deep inelastic context, the contribution strange quarks make to the proton spin is encapsulated in the helicity-difference strange quark parton distribution function,

$$\Delta s(x) = s^{\rightarrow}(x) - s^{\leftarrow}(x)$$

where $s^{\rightarrow}(x)$ $[s^{\leftarrow}(x)]$ is the probability density for finding a strange quark of momentum fraction x with its spin parallel [anti-parallel] to the proton spin. The axial current relates the first moment of this parton distribution function to the value of the strange quark contribution to the elastic axial form factor of the proton [91], G_A^s, at $Q^2 = 0$:

$$\int_0^1 dx \Delta s(x) = G_A^s(Q^2 = 0).$$

The strange quark contribution to the elastic axial form factor can be measured by combining data from neutrino NC elastic scattering from the proton with data from parity-violating elastic $\vec{e}p$ scattering [92]. In this way the strange quark spin contribution to the proton spin can be measured in a completely independent way using low-Q^2 elastic scattering instead of high-Q^2 deep inelastic scattering. An analysis done using this method [85] indicates that G_A^s may in fact be negative at $Q^2 = 0$ but this conclusion is not definitive due to the limitations of the currently available neutrino data.

Since the neutrino experiments will undoubtedly be carried out on nuclear targets (perhaps carbon or argon), then the extraction of the properties of the proton from these data needs to be done with care. Recent theoretical investigations point to the idea of measuring the ratio of NC to CC yields; nuclear effects appear to largely cancel in this ratio [93], leaving behind the ratio that would have been obtained on nucleon targets.

The only available data on neutrino NC elastic scattering is from the BNL E734 experiment [94]; the uncertainties reported from that experiment are considerable and limit the preciseness of any extraction of G_A^s based on them. If NuSOnG can provide more precise measurements of NC elastic scattering extended to lower Q^2 then the promise of this analysis technique can be fulfilled.

C. Measurements of the Charm Sea:

1. *Charm Production*

We can also study the charm sea component of the proton which can arise from the gluon splitting process $g \rightarrow c\bar{c}$ producing charm constituents inside the proton.[95, 96, 97] In a measurement complementary to the above strange sea extraction, the charm sea, $c(x, \mu)$, can be measured using the following process:

$$\begin{aligned} \nu_\mu + c \rightarrow \nu_\mu + \; & c \\ & \hookrightarrow s + \mu^+ + \nu_\mu \end{aligned} .$$

In this process, we excite a constituent charm quark in the proton via the NC exchange of a Z boson; the final state charm quark then decays semi-leptonically into $s\mu^+\nu_\mu$. We refer to this process as Wrong Sign Muon (WSM) production as the observed muon is typically the opposite sign from the expected $\nu_\mu d \rightarrow \mu^- u$ DIS process. For antineutrino beams, there is a complementary process $\bar{\nu}_\mu + \bar{c} \rightarrow \bar{\nu}_\mu + \bar{c}$ with a subsequent $\bar{c} \rightarrow \bar{s} + \mu^- + \bar{\nu}_\mu$ decay with yields a WSM with respect to the conventional $\bar{\nu}_\mu u \rightarrow \mu^+ d$ process. Here, the ability of NuSOnG to have sign-selected beams is crucial to this measurement as it allows us to distinguish the secondary muons, and thus extract the charm-sea component.

In the conventional implementation of the heavy quark PDFs, the charm quark becomes an active parton in the proton when the scale μ is greater than the charm mass m_c; *i.e.* $f_c(x, \mu)$ is nonzero for $\mu > m_c$. Additionally, we must "rescale" the Bjorken x variable as we have a massive charm in the final state. The original rescaling procedure is to make the substitution $x \rightarrow x(1+m_c^2/Q^2)$ which provides a kinematic penalty for producing the heavy charm quark in the final state.[98] As the charm is pair-produced by the $g \rightarrow c\,\bar{c}$ process, there are actually two charm quarks in the final state—one which is observed in the semi-leptonic decay, and one which decays hadronically and is part of the hadronic shower. Thus, the appropriate rescaling is not $x \rightarrow x(1 + m_c^2/Q^2)$ but instead $x \rightarrow \chi = x(1 + 4m_c^2/Q^2)$; this rescaling is implemented

in the ACOT–χ scheme, for example.[99, 100, 101] The factor $(1+4m_c^2/Q^2)$ represents a kinematic suppression factor which will suppress the charm process relative to the lighter quarks.

The differential cross section for NC neutrino scattering is

$$\frac{d\sigma}{d\xi dy}(\nu p \ \rightarrow \ \nu c) = \frac{G_F^2 M_N E_\nu}{\pi} R_Z^2(Q^2) \ \times \\ \times \ \left[g_L^2 + g_R^2(1-y)^2 - \frac{1}{2}(2 g_L g_R)\frac{M_N}{E_\nu}\right] \xi\, c(\xi,\mu),$$

where $g_L = t_3 - Q_c^2 \sin^2\theta_W$, $g_R = -Q_c^2 \sin^2\theta_W$, and for charm $t_3 = 1/2$ and $Q_c = 2/3$. The factor $R_Z(Q^2) = 1/(1+Q^2/M_Z^2)$ arises from the Z-boson propagator. The corresponding result for the anti-charm is given with the substitutions $g_L \leftrightarrow g_R$ and $c \leftrightarrow \bar{c}$.

In the limit we can neglect the M_N/E_ν term we have the approximate expressions for the total cross section:[96]

$$\sigma(\nu p \rightarrow \nu c) \sim \frac{G_F^2 M_N E_\nu}{\pi}(0.129)\, C \qquad (49)$$

and

$$\sigma(\nu p \rightarrow \nu \bar{c}) \sim \frac{G_F^2 M_N E_\nu}{\pi}(0.063)\, \bar{C} \qquad (50)$$

with $C = \int_{\xi_{min}}^1 \xi\, c(\xi,\mu)\, d\xi$ and $\bar{C} = \int_{\xi_{min}}^1 \xi\, \bar{c}(\xi,\mu)\, d\xi$. We take $\xi = x(1+4m_c^2/Q^2)$ and $\xi_{min} = m_c^2/(2M_N\nu)$.

We will be searching for the WSM signal compared to the conventional charged-current DIS process; therefore it is useful to benchmark the rate for WSM production by comparing this to the the usual charged-current DIS process,

$$\frac{d\sigma}{dx\, dy}(\nu p \ \rightarrow \ \mu^- X) = \frac{G_F^2 M_N E_\nu}{\pi} R_W^2(Q^2) \ \times \\ \times \ \left[q(x) + (1-y)^2 \bar{q}(x)\right] \qquad (51)$$

with $R_W(Q^2) = 1/(1+Q^2/M_W^2)$. We can again integrate over x and y to obtain an estimate of the total cross section in terms of the integrated PDFs as in Eq. (49) and Eq. (50):

$$\sigma(\nu N \ \rightarrow \ \mu^- X) \sim \frac{G_F^2 M_N E_\nu}{\pi} R_W^2(Q^2) \ \times \\ \times \ \frac{1}{2}\left[U + D + 2S + \frac{1}{3}(\bar{U} + \bar{D} + 2\bar{C})\right] \qquad (52)$$

where $\{U, D, S\}$ are defined analogously to C, and we have used $N = \frac{1}{2}(p+n)$ for an isoscalar target.

The relative rate for NC charm production is determined by the above factors together with a ratio of integrated PDFs. For a mean neutrino energy of 100 GeV, the massive charm cross section is down a factor of ~ 0.005 compared to the total inclusive cross section. As the muon from the NC charm process is a secondary muon, we must additionally fold in the semi-leptonic branching ratio $B_c \sim 10\%$, and the acceptance factor of observing the secondary muon in the detector (A_μ~20%).[17] Combining the relevant factors, we estimate the rate for NC charm production is approximately a factor of 10^{-4} as compared to the CC DIS process. Thus, for an anticipated design of 600M ν_μ CC events, one would expect on the order of 60K NC charm events. This estimate is also consistent with a direct scaling from the NuTeV result of Ref. [97].

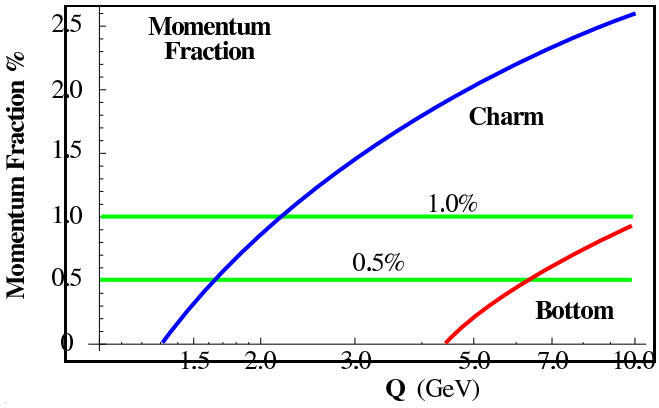

Figure 13: Integrated momentum fractions $\int_0^1 x\, f_i(x,Q)$ of charm (upper curve) and bottom (lower curve) PDFs (in percent) vs. Q in GeV. Both the quark and antiquark contributions are included. Horizontal lines at 0.5% and 1.0% are indicated as this is the typical size of postulated intrinsic contributions.

2. *Backgrounds*

Extrapolating from investigations by CCFR [96], and NuTeV [97], the dominant background for the measurement of the charm sea comes from $\bar{\nu}_\mu$ contamination. In these studies, it was determined that by demanding $E_{vis} > 100$ GeV, the background rate could be reduced to 2.3×10^{-4}. Other background processes include ν_e induced dilepton production, mis-identified dimuon events, and NC interactions with a π/K decay in the hadron shower; these processes contribute approximately an additional 1.5×10^{-4} to the background rate. As compared to CCFR and NuTeV, the NuSOnG design has a number of improvements such as lower mass density for improved shower measurement; hence, comparable background reductions should be achievable.

3. *Intrinsic Charm*

In the above discussion we have assumed that the charm component of the proton arises perturbatively

from gluons splitting into charm quark pairs, $g \to c\bar{c}$; in this scenario the charm PDF typically vanishes at scales below the charm mass ($f_c(x, \mu < m_c) = 0$), and for $\mu > m_c$ all the charm partons arise from gluon splitting.

There is an alternative picture where the charm quarks are taken to be intrinsic to the proton; in this case there are intrinsic charm partons present at scales $\mu < m_c$. For $\mu > m_c$, the charm PDF is then a combination of this "intrinsic" PDF and the "extrinsic" PDF component arising from the $g \to c\bar{c}$ process.

A number of analyses have searched for an intrinsic charm component of the proton, and this intrinsic component is typically constrained to have an integrated momentum fraction less than a percent or two [102, 103].

In Figure 13 we display the integrated momentum fraction, $\int_0^1 x\, f_i(x, \mu)$, for charm and bottom as a function of μ due to the "extrinsic" PDF component arising from the $g \to c\bar{c}$ or $g \to b\bar{b}$ process. These momentum fractions start from zero at the corresponding quark mass, and increase slowly as the partonic components pick up momentum from the gluon splitting process.

If we are searching for an additional intrinsic component with a momentum fraction of $\sim 1\%$, we will be most sensitive to such a component in the threshold region where the "intrinsic" component is not overwhelmed by the "extrinsic" contribution. In this regard, NuSOnG is well suited to search for these intrinsic terms as it will provide good statistics in the threshold region. Measuring the charm production process described above, NuSOnG can attempt to extract the charm PDF as a function of the μ scale, and then evolve back to $\mu = m_c$. Three outcomes are possible:

1. $f_c(x, \mu = m_c) < 0$, which would imply the data are inconsistent with the normal QCD evolution.[2]
2. $f_c(x, \mu = m_c) = 0$, which would imply the data is consistent with no intrinsic charm PDF.
3. $f_c(x, \mu = m_c) > 0$, which would imply the data is inconsistent with an intrinsic charm PDF.

By making accurate measurements of charm induced processes in the threshold region, NuSOnG can provide a discriminating test to determine which of the above possibilities is favored. Hence, the high statistics of NuSOnG in the threshold region are well suited to further constrain the question of an intrinsic charm component.

VIII. SUMMARY AND CONCLUSIONS

The NuSOnG experiment can search for "new physics" from the keV through TeV energy scales. This article has focused mainly on the QCD physics which can be accessed with this new high energy, high statistics neutrino scattering experiment. During its five-year data acquisition period, the NuSOnG experiment could record almost one hundred thousand neutrino-electron elastic scatters and hundreds of millions of deep inelastic scattering events, exceeding the current world data sample by more than an order of magnitude.

With this wealth of data, NuSOnG can address a wide variety of topics including the following.

- NuSOnG can increase the statistics of the Elastic Scattering (ES) and Deeply Inelastic Scattering (DIS) data sets by nearly two orders of magnitude.
- The unprecedented statistics of NuSOnG allow the possibility to perform separate extractions of the structure functions: $\{F_2^\nu, xF_e^\nu, R_L^\nu, F_2^{\bar{\nu}}, xF_e^{\bar{\nu}}, R_L^{\bar{\nu}}\}$. This allows us to test many of the symmetries and assumptions which were employed in previous structure function determinations.
- NuSOnG will help us to disentangle the nuclear effects which are present in the PDFs. Furthermore, this may help us address the long-standing tensions between the NC charged-lepton and CC neutrino DIS measurements.
- High precision NuSOnG measurements are sensitive to Charge Symmetry Violation (CSV) and other "new physics" processes. Such effects can significantly influence precision Standard Model parameter extractions such as $\sin\theta_W$. In particular, ΔxF_3 is a sensitive probe of both the heavy quark components, and CSV effects.
- NuSOnG dimuon production provides an exceptional probe of the strange quark PDFs, and the sign-selected beam can separately study $s(x)$ and $\bar{s}(x)$. Additionally, NuSOnG can probe the s-quark contribution to the proton spin.
- The high statistics of NuSOnG may allow the measurement of the charm sea and an method to prove the intrinsic-charm content of the proton. While this is a difficult measurement, the NuSOnG kinematics allow the measurement of charm-induced processes in the threshold region where the "intrinsic" character can most easily be discerned.

While the above list presents a very compelling physics case for NuSOnG, this is only a subset of the full range of investigations that can be addressed with this facility.

Acknowledgments

We thank the following people for their informative discussions regarding neutrino-nucleus interactions. and their thoughtful comments on the development of this

[2] If we work at NLO, $f_c(x, \mu = m_c)$ should be strictly greater than or equal to zero; at NNLO and beyond the boundary conditions yield a negative PDF of order $\sim \alpha_s^2$

physics case: Andrei Kataev, Sergey Kulagin, P. Langacker, Roberto Petti, M. Shaposhnikov, F. Vannucci, and J. Wells. We acknowledge the support of the following funding agencies for the authors of this paper: Deutsche Forschungsgemeinschaft, The Kavli Institute for Theoretical Physics, The United States Department of Energy, The United States National Science Foundation.

[1] E. A. Paschos and L. Wolfenstein. Tests for neutral currents in neutrino reactions. *Phys. Rev.*, D7:91–95, 1973.

[2] G. P. Zeller et al. A precise determination of electroweak parameters in neutrino nucleon scattering. *Phys. Rev. Lett.*, 88:091802, 2002, hep-ex/0110059.

[3] T. Adams et al. Terascale Physics Opportunities at a High Statistics, High Energy Neutrino Scattering Experiment: NuSOnG. *Int. J. Mod. Phys.*, A24:671–717, 2009, 0803.0354.

[4] William Glenn Seligman. A Next-to-leading order QCD analysis of neutrino - iron structure functions at the Tevatron. FERMILAB-THESIS-1997-21.

[5] M. Shaevitz. Private Communication.

[6] M. Arneodo et al. Measurement of the proton and deuteron structure functions, F2(p) and F2(d), and of the ratio σ_L/σ_T. *Nucl. Phys.*, B483:3–43, 1997, hep-ph/9610231.

[7] Un-Ki Yang et al. Extraction of $R = \sigma_L/\sigma_T$ from CCFR ν/μ-Fe and $\bar{\nu}/\bar{\mu}$-Fe differential cross sections. *Phys. Rev. Lett.*, 87:251802, 2001, hep-ex/0104040.

[8] Un-Ki Yang et al. Measurements of F_2 and $xF_3^{\nu} - xF_3^{\bar{\nu}}$ from CCFR ν_μ−Fe and $\bar{\nu}_\mu$−Fe data in a physics model independent way. *Phys. Rev. Lett.*, 86:2742–2745, 2001, hep-ex/0009041.

[9] Un-Ki Yang et al. Measurements of the longitudinal structure function and |V(cs)| in the CCFR experiment. 1998, hep-ex/9806023.

[10] Cynthia Kay McNulty. Measurements of R_L and V(CS) from the CCFR experiment. FERMILAB-THESIS-1997-61.

[11] T. Adams et al. Expression of Interest for Neutrinos Scattering on Glass: NuSOnG. The NuSOnG Expression of Interest is available at http://www-nusong.fnal.gov, 2007.

[12] R. Garoby. Upgrade Issues for the CERN Accelerator Complex. *Conf. Proc.*, C0806233:fryagm01, 2008.

[13] R. Garoby. Scenarios for upgrading the LHC injectors. Prepared for LHC LUMI 2006 CARE-HHH-APD Workshop, Valencia, Spain, 16-20 Oct 2006.

[14] Deborah A. Harris and A. Para. Neutrino oscillation appearance experiment using nuclear emulsion and magnetized iron. *Nucl. Instrum. Meth.*, A451:173–175, 2000, hep-ex/0001035.

[15] M. Tzanov et al. Precise measurement of neutrino and anti-neutrino differential cross sections. *Phys. Rev.*, D74:012008, 2006, hep-ex/0509010.

[16] L. W. Whitlow, Stephen Rock, A. Bodek, E. M. Riordan, and S. Dasu. A Precise extraction of $R = \sigma_L/\sigma_T$ from a global analysis of the SLAC deep inelastic *ep* and *ed* scattering cross-sections. *Phys. Lett.*, B250:193–198, 1990.

[17] A. O. Bazarko et al. Determination of the strange quark content of the nucleon from a next-to-leading order QCD analysis of neutrino charm production. *Z. Phys.*, C65:189–198, 1995, hep-ex/9406007.

[18] M. Tzanov et al. New QCD results from NuTeV. 2003, hep-ex/0306035.

[19] Bonnie T. Fleming et al. A first measurement of low x low Q^2 structure functions in neutrino scattering. *Phys. Rev. Lett.*, 86:5430–5433, 2001, hep-ex/0011094.

[20] G. Onengut et al. Measurement of nucleon structure functions in neutrino scattering. *Phys. Lett.*, B632:65–75, 2006.

[21] J. Gomez et al. Measurement of the A-dependence of deep inelastic electron scattering. *Phys. Rev.*, D49:4348–4372, 1994.

[22] B. L. Ioffe, Valery A. Khoze, and L. N. Lipatov. Hard Processes. Vol. 1: Phenomenology, Quark Parton Model. Amsterdam, Netherlands: North-holland (1984) 340p.

[23] Gunther Piller and Wolfram Weise. Nuclear deep-inelastic lepton scattering and coherence phenomena. *Phys. Rept.*, 330:1–94, 2000, hep-ph/9908230.

[24] B. Z. Kopeliovich and P. Marage. Low Q^2, high neutrino ν physics (CVC, PCAC, hadron dominance). *Int. J. Mod. Phys.*, A8:1513–1602, 1993.

[25] S. A. Kulagin. Nuclear shadowing in neutrino deep inelastic scattering. 1998, hep-ph/9812532.

[26] B. Badelek, M. Krawczyk, K. Charchula, and J. Kwiecinski. Small x physics in deep inelastic lepton hadron scattering. *Rev. Mod. Phys.*, 64:927–960, 1992.

[27] S. A. Kulagin and R. Petti. Neutrino inelastic scattering off nuclei. *Phys. Rev.*, D76:094023, 2007, hep-ph/0703033.

[28] R. J. Glauber and G. Matthiae. High-energy scattering of protons by nuclei. *Nucl. Phys.*, B21:135–157, 1970.

[29] J. F. Owens et al. The Impact of new neutrino DIS and Drell-Yan data on large-x parton distributions. *Phys. Rev.*, D75:054030, 2007, hep-ph/0702159.

[30] S. A. Kulagin and R. Petti. Global study of nuclear structure functions. *Nucl. Phys.*, A765:126–187, 2006, hep-ph/0412425.

[31] E. Reya. Perturbative Quantum Chromodynamics. *Phys. Rept.*, 69:195, 1981.

[32] Yuri L. Dokshitzer. Calculation of the Structure Functions for Deep Inelastic Scattering and e+ e- Annihilation by Perturbation Theory in Quantum Chromodynamics. (In Russian). *Sov. Phys. JETP*, 46:641–653, 1977.

[33] V. N. Gribov and L. N. Lipatov. Deep inelastic e p scattering in perturbation theory. *Sov. J. Nucl. Phys.*, 15:438–450, 1972.

[34] Guido Altarelli and G. Parisi. Asymptotic Freedom in Parton Language. *Nucl. Phys.*, B126:298, 1977.

[35] A. D. Martin, W. J. Stirling, R. S. Thorne, and G. Watt. Update of Parton Distributions at NNLO. *Phys. Lett.*, B652:292–299, 2007, 0706.0459.

[36] Pavel M. Nadolsky et al. Implications of CTEQ global analysis for collider observables. *Phys. Rev.*,

D78:013004, 2008, 0802.0007.

[37] I. Schienbein et al. Nuclear PDFs from neutrino deep inelastic scattering. *Phys. Rev.*, D77:054013, 2008, 0710.4897.

[38] M. Gluck, E. Reya, and A. Vogt. Dynamical parton distributions revisited. *Eur. Phys. J.*, C5:461–470, 1998, hep-ph/9806404.

[39] C. Boros, Fernando Monti Steffens, J. T. Londergan, and Anthony William Thomas. A new analysis of charge symmetry violation in parton distributions. *Phys. Lett.*, B468:161–167, 1999, hep-ph/9908280.

[40] Richard D. Ball, Deborah A. Harris, and Kevin S. McFarland. Flavor decomposition of nucleon structure at a neutrino factory. 2000, hep-ph/0009223.

[41] S. Kretzer, Fredrick I. Olness, R. J. Scalise, R. S. Thorne, and Un-Ki Yang. Predictions for neutrino structure functions. *Phys. Rev.*, D64:033003, 2001, hep-ph/0101088.

[42] Alan D. Martin, R. G. Roberts, W. J. Stirling, and R. S. Thorne. MRST2001: Partons and α_s from precise deep inelastic scattering and Tevatron jet data. *Eur. Phys. J.*, C23:73–87, 2002, hep-ph/0110215.

[43] C. Boros, J. T. Londergan, and Anthony William Thomas. Evidence for charge symmetry violation in parton distributions. *Phys. Rev.*, D59:074021, 1999, hep-ph/9810220.

[44] C. Boros, J. T. Londergan, and Anthony William Thomas. Evidence for substantial charge symmetry violation in parton distributions. *Phys. Rev. Lett.*, 81:4075–4078, 1998, hep-ph/9806249.

[45] A. Baldit et al. Study of the isospin symmetry breaking the in the light quark sea of the nucleon from the Drell-Yan process. *Phys. Lett.*, B332:244–250, 1994.

[46] A. D. Martin, R. G. Roberts, W. J. Stirling, and R. S. Thorne. Parton distributions incorporating QED contributions. *Eur. Phys. J.*, C39:155–161, 2005, hep-ph/0411040.

[47] Markus Roth and Stefan Weinzierl. QED corrections to the evolution of parton distributions. *Phys. Lett.*, B590:190–198, 2004, hep-ph/0403200.

[48] M. Gluck, P. Jimenez-Delgado, and E. Reya. Radiatively generated isospin violations in the nucleon and the NuTeV anomaly. *Phys. Rev. Lett.*, 95:022002, 2005, hep-ph/0503103.

[49] F. Abe et al. Measurement of the lepton charge asymmetry in W boson decays produced in $p\bar{p}$ collisions. *Phys. Rev. Lett.*, 81:5754–5759, 1998, hep-ex/9809001.

[50] A. Bodek, Q. Fan, M. Lancaster, K. S. McFarland, and Un-Ki Yang. Implication of W boson charge asymmetry measurements in $p\bar{p}$ collisions to models for charge symmetry violations in parton distributions. *Phys. Rev. Lett.*, 83:2892–2895, 1999, hep-ex/9904022.

[51] J. Pumplin et al. New generation of parton distributions with uncertainties from global QCD analysis. *JHEP*, 07:012, 2002, hep-ph/0201195.

[52] D. Allasia et al. Measurement of the neutron and the proton F2 structure function ratio. *Phys. Lett.*, B249:366–372, 1990.

[53] E. A. Hawker et al. Measurement of the light antiquark flavor asymmetry in the nucleon sea. *Phys. Rev. Lett.*, 80:3715–3718, 1998, hep-ex/9803011.

[54] Stanley J. Brodsky, Ivan Schmidt, and Jian-Jun Yang. Nuclear antishadowing in neutrino deep inelastic scattering. *Phys. Rev.*, D70:116003, 2004, hep-ph/0409279.

[55] M. Goncharov et al. Precise measurement of dimuon production cross-sections in ν/μ-Fe and $\bar{\nu}/\bar{\mu}$-Fe deep inelastic scattering at the Tevatron. *Phys. Rev.*, D64:112006, 2001, hep-ex/0102049.

[56] P. Vilain et al. Leading-order QCD analysis of neutrino induced dimuon events. *Eur. Phys. J.*, C11:19–34, 1999.

[57] P. Astier et al. Neutrino production of opposite sign dimuons in the NOMAD experiment. *Phys. Lett.*, B486:35–48, 2000.

[58] G. P. Zeller et al. On the effect of asymmetric strange seas and isospin- violating parton distribution functions on $\sin^2\theta_W$ measured in the NuTeV experiment. *Phys. Rev.*, D65:111103, 2002, hep-ex/0203004.

[59] V. Barone, C. Pascaud, and F. Zomer. A new global analysis of deep inelastic scattering data. *Eur. Phys. J.*, C12:243–262, 2000, hep-ph/9907512.

[60] Kevin S. McFarland and Sven-Olaf Moch. Conventional physics explanations for the NuTeV $\sin^2\theta_W$. 2003, hep-ph/0306052.

[61] S. Davidson, S. Forte, P. Gambino, N. Rius, and A. Strumia. Old and new physics interpretations of the NuTeV anomaly. *JHEP*, 02:037, 2002, hep-ph/0112302.

[62] F. Olness et al. Neutrino dimuon production and the strangeness asymmetry of the nucleon. *Eur. Phys. J.*, C40:145–156, 2005, hep-ph/0312323.

[63] D. Mason et al. Measurement of the Nucleon Strange-Antistrange Asymmetry at Next-to-Leading Order in QCD from NuTeV Dimuon Data. *Phys. Rev. Lett.*, 99:192001, 2007.

[64] P. H. Sandler et al. Hadron shower punchthrough and muon production by hadrons of 40-GeV, 70-GeV and 100-GeV. *Phys. Rev.*, D42:759–770, 1990.

[65] P. H. Sandler et al. Neutrino production of same sign dimuons at the Fermilab Tevatron. *Z. Phys.*, C57:1–12, 1993.

[66] Pamela Helen Sandler. Neutrino production of same sign dimuons at the Fermilab tevatron. RX-1381 (WISCONSIN).

[67] S. A. Rabinowitz et al. Measurement of the strange sea distribution using neutrino charm production. *Phys. Rev. Lett.*, 70:134–137, 1993.

[68] H. Abramowicz et al. Experimental Study of Opposite Sign Dimuons Produced in Neutrino and anti-neutrinos Interactions. *Z. Phys.*, C15:19, 1982.

[69] Tim Bolton. Determining the CKM parameter V(cd) from νN charm production. 1997, hep-ex/9708014.

[70] A. Kayis-Topaksu et al. Determination of the semileptonic branching fraction of charm hadrons produced in neutrino charged-current interactions. *Phys. Lett.*, B549:48–57, 2002.

[71] G. Barichello et al. Performance of the NOMAD-STAR detector. *Nucl. Instrum. Meth.*, A506:217–237, 2003.

[72] Malcolm Ellis and F. J. P. Soler. Charm identification using silicon detectors in a neutrino experiment. *J. Phys.*, G29:1975–1979, 2003.

[73] B. Mueller et al. Measurement of the proton's neutral weak magnetic form factor. *Phys. Rev. Lett.*, 78:3824–3827, 1997, nucl-ex/9702004.

[74] R. Hasty et al. Strange magnetism and the anapole structure of the proton. *Science*, 290:2117, 2000, nucl-ex/0102001.

[75] D. T. Spayde et al. The strange quark contribution to the proton's magnetic moment. *Phys. Lett.*, B583:79–86, 2004, nucl-ex/0312016.

[76] T. M. Ito et al. Parity-violating electron deuteron scattering and the proton's neutral weak axial vector form factor. *Phys. Rev. Lett.*, 92:102003, 2004, nucl-ex/0310001.

[77] K. A. Aniol et al. Parity-violating electroweak asymmetry in $\vec{e}p$ scattering. *Phys. Rev.*, C69:065501, 2004, nucl-ex/0402004.

[78] F. E. Maas et al. Measurement of strange quark contributions to the nucleon's form factors at $Q^2 = 0.230$-$(GeV/c)^2$. *Phys. Rev. Lett.*, 93:022002, 2004, nucl-ex/0401019.

[79] F. E. Maas et al. Evidence for strange quark contributions to the nucleon's form factors at $Q^2 = 0.108$-$(GeV/c)^2$. *Phys. Rev. Lett.*, 94:152001, 2005, nucl-ex/0412030.

[80] D. S. Armstrong et al. Strange quark contributions to parity-violating asymmetries in the forward G0 electron proton scattering experiment. *Phys. Rev. Lett.*, 95:092001, 2005, nucl-ex/0506021.

[81] A. Acha et al. Precision Measurements of the Nucleon Strange Form Factors at $Q^2 \sim 0.1\,\mathrm{GeV}^2$. *Phys. Rev. Lett.*, 98:032301, 2007, nucl-ex/0609002.

[82] K. A. Aniol et al. Constraints on the nucleon strange form factors at $Q^2 \sim 0.1\,\mathrm{GeV}^2$. *Phys. Lett.*, B635:275–279, 2006, nucl-ex/0506011.

[83] K. A. Aniol et al. Parity-violating electron scattering from He-4 and the strange electric form factor of the nucleon. *Phys. Rev. Lett.*, 96:022003, 2006, nucl-ex/0506010.

[84] M. J. Musolf et al. Intermediate-energy semileptonic probes of the hadronic neutral current. *Phys. Rept.*, 239:1–178, 1994.

[85] Stephen F. Pate, David W. McKee, and Vassili Papavassiliou. Strange Quark Contribution to the Vector and Axial Form Factors of the Nucleon: Combined Analysis of G0, HAPPEx, and Brookhaven E734 Data. *Phys. Rev.*, C78:015207, 2008, 0805.2889.

[86] Jianglai Liu, Robert D. McKeown, and Michael J. Ramsey-Musolf. Global Analysis of Nucleon Strange Form Factors at Low Q^2. *Phys. Rev.*, C76:025202, 2007, 0706.0226.

[87] Ross Daniel Young, Julie Roche, Roger D. Carlini, and Anthony William Thomas. Extracting nucleon strange and anapole form factors from world data. *Phys. Rev. Lett.*, 97:102002, 2006, nucl-ex/0604010.

[88] Elliot Leader, Aleksander V. Sidorov, and Dimiter B. Stamenov. Longitudinal polarized parton densities updated. *Phys. Rev.*, D73:034023, 2006, hep-ph/0512114.

[89] A. Airapetian et al. Measurement of Parton Distributions of Strange Quarks in the Nucleon from Charged-Kaon Production in Deep-Inelastic Scattering on the Deuteron. *Phys. Lett.*, B666:446–450, 2008, 0803.2993.

[90] Daniel de Florian, Rodolfo Sassot, Marco Stratmann, and Werner Vogelsang. Global Analysis of Helicity Parton Densities and Their Uncertainties. *Phys. Rev. Lett.*, 101:072001, 2008, 0804.0422.

[91] M. Anselmino, A. Efremov, and E. Leader. The theory and phenomenology of polarized deep inelastic scattering. *Phys. Rept.*, 261:1–124, 1995, hep-ph/9501369.

[92] Stephen F. Pate. Determination of the strange form factors of the nucleon from νp, $\bar{\nu} p$, and parity-violating $\vec{e}p$ elastic scattering. *Phys. Rev. Lett.*, 92:082002, 2004, hep-ex/0310052.

[93] N. Jachowicz, P. Vancraeyveld, P. Lava, C. Praet, and J. Ryckebusch. Strangeness content of the nucleon in quasielastic neutrino-nucleus reactions. *Phys. Rev.*, C76:055501, 2007, 0708.4135.

[94] L. A. Ahrens et al. Measurement of Neutrino - Proton and anti-neutrino - Proton Elastic Scattering. *Phys. Rev.*, D35:785, 1987.

[95] Janet M. Conrad, Michael H. Shaevitz, and Tim Bolton. Precision measurements with high energy neutrino beams. *Rev. Mod. Phys.*, 70:1341–1392, 1998, hep-ex/9707015.

[96] S. R. Mishra et al. A study of wrong sign single muon production in muon- neutrino - nucleon interaction. *Z. Phys.*, C44:187, 1989.

[97] A. Alton et al. Observation of neutral current charm production in ν_μFe scattering at the Fermilab Tevatron. *Phys. Rev.*, D64:012002, 2001.

[98] R. Michael Barnett. Evidence for New Quarks and New Currents. *Phys. Rev. Lett.*, 36:1163–1166, 1976.

[99] J. Amundson, Fredrick I. Olness, C. Schmidt, W. K. Tung, and X. Wang. Theoretical description of heavy quark production in DIS. To be published in the proceedings of 6th International Workshop on Deep Inelastic Scattering and QCD (DIS 98), Brussels, Belgium, 4-8 Apr 1998.

[100] James Amundson, Carl Schmidt, Wu-Ki Tung, and Xiaoning Wang. Charm production in deep inelastic scattering from threshold to high Q^2. *JHEP*, 10:031, 2000, hep-ph/0005221.

[101] Wu-Ki Tung, Stefan Kretzer, and Carl Schmidt. Open heavy flavor production in QCD: Conceptual framework and implementation issues. *J. Phys.*, G28:983–996, 2002, hep-ph/0110247.

[102] B. W. Harris, J. Smith, and R. Vogt. Reanalysis of the EMC charm production data with extrinsic and intrinsic charm at NLO. *Nucl. Phys.*, B461:181–196, 1996, hep-ph/9508403.

[103] J. Pumplin, H. L. Lai, and W. K. Tung. The Charm Parton Content of the Nucleon. *Phys. Rev.*, D75:054029, 2007, hep-ph/0701220.